Assessing the performance of climate change simulation results from BESM-OA2.5 in comparison to a CMIP5 model ensemble

Vinicius Buscioli Capistrano[1,2], Paulo Nobre[1], Renata Tedeschi[1], Josiane Silva[1], Marcus Bottino[1], Manoel Baptista da Silva Junior[1], Otacílio Leandro Menezes Neto[1], Silvio Nilo Figueroa[1], José Paulo Bonatti[1], Paulo Yoshio Kubota[1], Julio Pablo Reyes Fernandez[1], Emanuel Giarolla[1], Jessica Vial[3], and Carlos A. Nobre[4]

[1]Center for Weather Forecast and Climate Studies/National Institute for Space Research (CPTEC/INPE), Cachoeira Paulista – São Paulo, Brazil
[2]Amazonas State University (UEA), Manaus – Amazonas, Brazil.
[3]Laboratoire de Météorologie Dynamique/Centre National de la Recherche Scientifique (LMD/CNRS), Paris, France
[4]National Center for Monitoring and Early Warning of Natural Disasters (CEMADEN), São José dos Campos – São Paulo, Brazil

Correspondence: Vinicius Buscioli Capistrano, Amazonas State University, 1200 Darcy Vargas Ave., 69050-020, Manaus – Amazonas, Brazil (vcapistrano@uea.edu.br)

Abstract. The main features of climate change patterns, as simulated by the coupled ocean-atmosphere version 2.5 of the Brazilian Earth System Model (BESM-OA2.5) are contrasted with those of other 25 CMIP5 models, focusing on temperature, precipitation and atmospheric circulation. The climate sensitivity to quadrupling atmospheric CO_2 concentration is investigated from two techniques: the linear regression (Gregory et al., 2004) and Radiative Kernel (Soden and Held, 2006; Soden et al., 2008) methods. Radiative kernels from both NCAR and GFDL are used in order to decompose the climate feedback responses of CMIP5 models and BESM-OA2.5 into different processes. Applying the linear regression method for equilibrium climate sensitivity (ECS) estimation, we obtain a value for BESM close to the ensemble mean value. The study reveals that BESM has shown zonally averaged feedbacks estimated from Radiative Kernel within the ensemble standard deviation of the other CMIP5 models. The exceptions are found in the high-latitudes of the Northern Hemisphere and the ocean near Antarctic, where BESM shows values for lapse-rate, humidity feedbacks and albedo marginally out of the standard deviation of CMIP5 multi-model ensemble. For those areas, BESM also presented an strong positive cloud feedback being a outlier comparatively to all analyzed models. Moreover, BESM shows physically consistent changes in the pattern of temperature, precipitation and atmospheric circulation.

1 Introduction

The effects of increased atmospheric CO_2 concentration on the climate system has been studied over the last 120 years (Arrhenius, 1896; Callendar, 1938; Plass, 1956; Kaplan, 1960; Manabe and Wetherald, 1967, 1975; Manabe and Stouffer, 1980; IPCC, 2007, 2013; Pincus et al., 2016; Good et al., 2016, and many others). The human induced increase of atmospheric greenhouse gas (GHG) concentrations, sometimes given as the CO_2-equivalent concentration, contributes to a radiation imbalance at the Top-Of-Atmosphere (TOA), causing less outgoing radiation to leave the Earth System. The trapping of infrared radiation results in temperature rise at the lower levels of the troposphere, as well as an increase in ocean heating content. In addition, the increased GHG concentration can act as a trigger for climate feedback processes that will either amplify or damp the initial radiative perturbation (Cubasch and Cess, 1990). Earth system models (ESM) are the most advanced tools available for analyzing the coupled climate system (atmosphere, ocean, land, and ice) physical processes and their interactions, although they still exhibit important uncertainties in their projections of climate change (IPCC, 2013).

The equilibrium global-mean surface temperature change induced by doubling the CO_2 concentration in the atmosphere, referred to as the Equilibrium Climate Sensitivity (ECS), remains a centrally important measure of a model's climate response to CO_2 forcing. In the fifth Intergovernmental Panel on Climate Change (IPCC) assessment report (AR5), climate model estimates of the ECS range from 2 K to 4.5 K. For more than 40 years, this inter-model spread has been considered one of the most critical uncertainties for the evaluation of future climate changes (IPCC, 2013). This inter-model dispersion arises principally from differences in how climate models simulate climate feedback processes. Among them, the cloud feedback constitutes the largest source of spread for climate sensitivity estimates (Cess et al., 1989, 1990; Dufresne and Bony, 2008; Vial et al., 2013; Caldwell et al., 2016).

Beyond ECS, the response of precipitation to anthropogenic GHG emissions is a topic of great interest in climate science, given the potential consequences on both societies and ecosystems. Changes in precipitation can generally be decomposed into two processes: a thermodynamic component due to increased moisture and no circulation change, and a dynamic component due to circulation change and no moisture change (Bony et al., 2006; Seager et al., 2010). The thermodynamic component gives rise to the well-known 'wet-gets-wetter' and 'dry-gets-drier' pattern of precipitation changes described by Held and Soden (2006), which is associated with Clausius-Clapeyron relation (saturation-specific humidity increase exponentially with temperature) (Marvel and Bonfils, 2013). As to the dynamic component associated with circulation change, it sometimes yields strong deviations from the thermodynamic pattern of precipitation, and is known to dominate the uncertainty in total precipitation due to uncertainties in the regional circulation change (Xie et al., 2015).

The recent development of the Brazilian Earth System Model, ocean-atmosphere coupled version 2.5 (BESM-OA2.5) is an evolution of BESM-OA2.3 first presented by Nobre et al. (2013). The authors scrutinized the BESM-OA2.3 model behavior for decadal climate variability and climate change using extended runs with ensemble members totaling over 2000 years of model simulations. El Niño/Southern Oscillation (ENSO) interannual variability over the equatorial Pacific and the inter-hemispheric gradient mode over the tropical Atlantic on decadal time scale are reproduced by BESM-OA2.3. Veiga et al. (2018) showed

that BESM-OA2.5 is able to simulate the general mean present-day climate state, as well as to reproduce the main climate variability, particularly over the Atlantic.

Here, we assess the main features of climate change patterns as simulated by BESM-OA2.5, with a focus on temperature (climate sensitivity and feedbacks), precipitation and atmospheric circulation. The recent development of the BESM-OA2.5 is a coordinated effort of the National Institute for Space Research (INPE) in Brazil in order to advance the understanding of the causes of the global and regional climate changes and their impacts on the socioeconomic sector. We evaluate how BESM's simulated climate change compares with Coupled Model Intercomparison Project phase 5 (CMIP5) models, discussing peculiarity of BESM climate response. The paper is structured as follows: section 2 presents the description of the new features of BESM2-OA2.5; section 3 presents the methodology, the results are presented in section 4; and section 5 presents the summary and conclusions.

2 Model Description

2.1 BESM-OA2.5

The coupled model BESM-OA2.5 is the result of coupling the Center for Weather Forecast and Climate Studies (CPTEC/INPE) Brazilian Atmospheric Model [BAM (Figueroa et al., 2016)] and the Geophysical Fluid Dynamics Laboratory (GFDL) Modular Ocean Model version 4p1 (Griffies et al., 2004) via the Flexible Modular System (FMS) also from GFDL. The dynamical core and physical processes of the atmospheric component of BESM-OA2.5 is the same that used by Veiga et al. (2018). BAM is a hydrostatic model, which its dynamical core is based on the spectral transform method which employs the global spherical harmonic basis functions. The Eulerian Advection scheme option is used in this study but with two-time-level semi-Lagrangian scheme for the transport of moisture and microphysics prognostic variables, which are carried out completely on the model grid space. Simplified fast physical parametrizations are used here due to computationally efficiency requirements for long integrations in comparison that used in the operational Numerical Weather Prediction (NWP) model. The summary of the main differences in physical processes between BAM used in this paper and BAM NWP operational is listed in Table 1. The dynamical equations in BAM are discretized following a spectral transform with horizontal resolution truncated at triangular wavenumber 62 (approximately an equivalent grid size of 1.875°) and 28 layers unevenly spaced in the vertical sigma coordinate with the top level at around 2.73 hPa. The oceanic component uses a tripolar grid at horizontal resolution of 1° in longitude, and in the latitudinal direction the grid spacing is 1/4° between 10°S-10°N, decreasing uniformly to 1° at 45° and to 2° at 90° in both hemispheres. The ocean grid has 50 vertical levels with a 10-m resolution in the upper 220 m, decreasing gradually to about 370 m at deeper levels.

Veiga et al. (2018) showed that BESM-OA2.5 is able to simulate the general mean climate state. However, substantial biases appear at the simulation associated with double ITCZ over the Pacific and Atlantic Oceans and regional biases in the precipitation over the Amazon and Indian regions. It is worth noting that BESM-OA2.5 shows improvement in ITCZ representation in comparison with the previews version (Nobre et al., 2013). BESM-OA2.5 also is capable to reproduce the most important large-scale interannual and decadal climate variabilities. The Atlantic Meridional Mode (Nobre and Srukla,

1996) is well simulated by the model in term of the spatial pattern and temporal variability, whereas this mode is poorly represented in most CMIP5 models (IPCC, 2013; Liu et al., 2013; Richter et al., 2014; Amaya et al., 2017). The Atlantic Meridional Overturning Circulation (AMOC) represented by BESM-OA2.5 has a mean circulation which is similar to the ensemble AMOC simulated by the CMIP5 models, but slightly lower than the averaged value based on observation. Moreover, the spatial structure of both the North Atlantic Oscilation (NAO) and the Pacific Decadal Oscillation (PDO) variability is well captured (Veiga et al., 2018).

2.2 Comparison to previous version

The main differences between BESM-OA2.5 and the previous version BESM-OA2.3 described in Nobre et al. (2013) are in the atmospheric model and how some surface layer variables are estimated, which are important in the coupling between atmosphere and ocean. The total energy balance at the TOA is better represented in BESM-OA2.5 than in BESM-OA2.3, which results in an improvement that reduced to around -4 W m^{-2} the mean global bias of -20 W m^{-2} presented by the latter. It should be noted that BESM-OA2.5 has a new set of parameterizations, mainly regarding a better microphysical processes representation. For instance, the previous model precipitation was parameterized only in terms of the large scale condensation. Moreover, BESM-OA2.5 underwent improvements in the representation of the wind, humidity and temperature in the surface layer, with the use of the similarity functions formulation presented by Jiménez et al. (2012). Based on Monin-Obukhov theory, the wind (u_{10m}), humidity (q_{2m}) and temperature (θ_{2m}) are estimated from the values of the first atmospheric model level and the surface, as described in Eq. (24), (25) and (26) of Jiménez et al. (2012). Furthermore, the similarity functions ψ_m and ψ_h depend on the stability regimes (Businger et al., 1971). For BESM-OA2.5, those regimes are associated with stable ($\zeta/L > 0$) and unstable ($\zeta/L \leq 0$) conditions (Arya, 1988). Those diagnostic variables are important for BESM because they are used in ocean-atmosphere coupling strategy.

One year long global simulations and 6 hourly outputs were done with BAM configured with surface layer schemes based on Arya (1988) and Jiménez et al. (2012), here called BAM-Arya (the original scheme) and BAM-Jimenez (the new scheme), respectively. The normalized root mean square error (RMSE) was computed with respect to the reanalysis NCEP-DOE (National Centers for Environmental Prediction – Department of Energy) version 2 (Kanamitsu et al., 2002). The normalized RMSE of the wind at 10 m, temperature and humidity at 2 m for the two surface layer schemes were investigated. Consistent improvements of BAM-Jimenez relative to BAM-Arya were noted in all the three variables over the oceanic regions. The normalized RMSE analysis over the continents presented less consistent results, with improved BAM-Jimenez representation of both winds and temperature, but degraded representation of the humidity field (figures not shown).

3 Methodology

3.1 Experiments design

For the purpose of this study, climate simulations are performed using BESM-OA2.5 (hereinafter BESM) for the piControl (pre-industrial control scenario, run for 300 years with atmospheric CO_2 concentration invariant at 274 ppmv) and abrupt4xCO_2 (run for 150 years after the abrupt quadrupling of atmospheric CO_2 at year 150 of the piControl simulation) scenarios, which means a spin-up of 150 years. These two scenarios that are commonly employed in CMIP5 studies for climate change assessment (Taylor et al., 2012; Eyring et al., 2016). Climate change is evaluated from the difference between the abrupt4xCO2 and piControl experiments. In addition, BESM's results are compared with a selection of 25 CMIP5 models listed in Table 2. All models, including BESM, are interpolated at 2.5° x 2.5° longitude/latitude horizontal resolution. All CMIP5 models data are available in the Earth System Grid Federation (ESGF).

3.2 Estimates of climate change sensitivity

Here we estimate the climate feedback using two different techniques: regression (Gregory et al., 2004) and Radiative Kernel (Soden et al., 2004, 2008) methods. The Gregory method has a more straightforward computation, however it returns only a global-mean value. On the other hand, it is possible to obtain the seasonal feedback for every lat-lon point with Radiative Kernel method, besides the feedback can be decomposed into different processes. Moreover, with the linear regression method, it is possible to estimate the ECS.

3.2.1 Linear forcing-feedback regression analysis

The regression method to compute the thermal response to radiative forcing is applied for 26 CMIP5 models including BESM. The method consists of the linear regression between the annual change (considering abrupt4xCO2 minus piControl) of the global-mean near-surface temperature (ΔT_{as}) and the net radiation change (ΔR) at TOA.

If G is the radiative forcing imposed on the climate system (here, associated with an abrupt increase in atmospheric CO_2 concentration) and ΔR the resulting radiative imbalance in the global-mean net radiative budget at TOA, then at any time, the response of the climate system to this radiative imbalance responds to the radiative forcing according to the following equation:

$$\Delta R = \lambda \Delta \overline{T}_{as} + G \tag{1}$$

where λ (< 0) is the climate feedback parameter and $\Delta \overline{T}_{as}$ the global-mean near-surface temperature change. In a sufficiently long simulation (coupled atmosphere-ocean models take millennia), when the climate system reaches a new equilibrium (ΔR = 0). For this method the ECS can be estimated as $\mathrm{ECS} = -G/\lambda$ in a shorter simulation (typically of 150 year) without reach the thermodynamical equilibrium. As the ECS is the theoretical equilibrium temperature for doubling CO2, in a quadrupling of CO2 it is necessary to divide its result by 2 (Andrews et al., 2012).

By using this linear forcing-response framework, we can estimate climate sensitivity, radiative forcing, and feedback parameter following the method proposed by Gregory et al. (2004). The values of λ (slope) and G (y-intercept) are estimated through the ordinary least square regression of the global-annual-mean of ΔR against $\Delta\overline{T}_{as}$ in all-sky conditions. Using the same linear technique, we decompose the feedback parameter into shortwave (SW) and longwave (LW) radiation components and we extract the clear sky radiative flux components from the BESM and CMIP data bases in order to estimate the cloud radiative forcing or cloud radiative effect ($\Delta\mathrm{CRE}$) defined as the difference between the all-sky and clear-sky feedback parameters (Andrews et al., 2012). Estimates of G, λ, $\Delta\mathrm{CRE}$, and ECS for all models are presented in the next section.

3.2.2 Climate feedbacks (Radiative Kernel)

The radiative kernel technique [as in Soden and Held (2006), Soden et al. (2008), Vial et al. (2013)] is used next to partition the feedback parameter λ into contributions from the temperature response (λ_T), water vapor ($\lambda_{\mathrm{ln}q}$), surface albedo (λ_a), and cloud (λ_c) feedbacks plus a residual term Re (Vial et al., 2013), and expressed in Eq. (2).

$$\lambda = \lambda_T + \lambda_{\mathrm{ln}q} + \lambda_a + \lambda_c + \mathrm{Re} \tag{2}$$

It is worth noting that in the regression method the radiative feedback is consistent with the actual radiative transfer scheme used in the climate model, while in the radiative kernel the feeckback is not integraly consistent. In fact, the kernel is obtained from another climate model that is not among the models analyzed. Model intercomparison is easily achieved using this method as the same kernel can be applied to all models (Soden and Held, 2006; Soden et al., 2008, 2018). This however assumes that the kernel is independent of models and climate states and that uncertainties in the radiative transfer code used to compute them are small compared to the models' climate responses (Soden et al., 2008).

Following Vial et al. (2013), we decompose the total feedback parameter (λ) into contributions from λ_T, $\lambda_{\mathrm{ln}q}$, λ_a, and λ_c as:

$$\begin{aligned}
\lambda &= \sum_x \lambda_x + \mathrm{Re} = \sum_x \frac{\partial R}{\partial x}\frac{dx}{d\overline{T}_{as}} + \mathrm{Re} = \sum_x K_x \frac{dx}{d\overline{T}_{as}} + \mathrm{Re} \\
\lambda &= \left(K_{T_s}\frac{dT_s}{d\overline{T}_{as}} + K_T\frac{dT}{d\overline{T}_{as}}\right) + \left(K_{\mathrm{ln}q}\frac{d\mathrm{ln}q}{d\overline{T}_{as}}\right) \\
&\quad + \left(K_a\frac{da}{d\overline{T}_{as}}\right) + \lambda_c + \mathrm{Re}
\end{aligned} \tag{3}$$

where the temperature feedback has been separated into the Planck feedback (vertically uniform tropospheric warming equal the surface warming) and lapse rate feedback (deviation from the tropospheric uniform warming):

$$\begin{aligned}
\lambda_T = \lambda_p + \lambda_{lr} &= \left(K_{T_s}\frac{dT_s}{d\overline{T}_{as}} + K_T\frac{dT_s}{d\overline{T}_{as}}\right) \\
&\quad + \left(K_T\frac{dT}{d\overline{T}_{as}} - K_T\frac{dT_s}{d\overline{T}_{as}}\right)
\end{aligned} \tag{4}$$

and where the water vapor feedback is computed assuming constant relative humidity (Soden et al., 2008; Shell et al., 2008; Jonko et al., 2013).

In Eq. (3), K_x (the radiative kernel for a variable x) and x [temperature (T_s and T, in K), natural logarithm of humidity ($\ln q$, in kg/kg) and albedo (a, dimensionless)] are function of longitude, latitude, and pressure vertical coordinates in monthly climatology. To obtain tropospheric averages, the water vapor and temperature feedbacks are vertically integrated from surface up to the tropopause, defined as being 100 hPa in the Equator, and varying linearly to 300 hPa in the Poles. The stratospheric temperature and water changes is not accounted for calculating the feedbacks, and they are shifted to the residuum.

We used both GFDL and National Center for Atmospheric Research (NCAR) radiative kernels to estimate climate feedbacks. More details on how the radiative kernels are obtained can be found in Soden et al. (2008) and Shell et al. (2008).

Due to the non-linearities involving clouds and net radiation at TOA (Soden et al., 2008), the cloud feedback is not calculated directly from these radiative kernels, which represents one of the key limitations of the kernel method. Instead, the cloud feedback is approximated using the cloud radiative forcing ($\Delta\mathrm{CRE}$) corrected for non-cloud feedbacks as in Soden et al. (2004, 2008). After the calculation of non-cloud feedbacks for both all-sky and clear-sky (superscript cs) conditions, we thus estimate the cloud feedback (λ_c) as:

$$\begin{aligned}
\Delta\mathrm{CRE} &= \Delta R - \Delta R^{cs} \\
\Delta\mathrm{CRE}_k &= (G - G^{cs})_{CO_2} - \Delta\overline{T}_{as} \sum_x (\lambda_x - \lambda_x^{cs}) \\
\Delta\mathrm{CRE}_a &= \Delta\mathrm{CRE} - \Delta\mathrm{CRE}_k \\
\lambda_c &= \frac{\Delta\mathrm{CRE}_a}{\overline{T}_{as}}
\end{aligned} \tag{5}$$

Where, ΔR^{cl} is the clear-sky net radiation flux at TOA. Following Soden et al. (2008), $(G - G_{cl})_{CO_2}$ was considered being equal to 2x0.69 W m^{-2} . Finally, a 30-year mean relative to the period from 120th to 150th year of each scenario was used for all feedbacks estimation.

3.3 Changes in the atmospheric circulation and precipitation

Monthly mean climatologies are computed for the last 30 years of piControl and abrupt4xCO2 runs, and the projected climate response to CO_2 increase is evaluated from the difference between these abrupt4xCO2 and piControl monthly mean climatologies. The statistical significance of this difference is calculated based on the t-Student test. The significance level used is of 90%. Furthermore, in order to evaluate how similar two spatial pattern are, we used the spatial inner product calculated as $\sum(A_i \cdot B_i)/(|A| \cdot |B|)$, where A and B are the 2-D variables and i is the spatial index related to their lat-lon coordinates.

4 Results

4.1 G, λ, $\Delta\mathrm{CRE}$ and ECS estimated by Gregory method

Figure 1 shows the linear regressions of ΔR , ΔLW (clear-sky) and ΔSW (clear-sky) against $\Delta\overline{T}_{as}$ for BESM. These linear regressions based on all-sky data are used to estimate ECS, G and λ, here in Figure 1 the regressions are also based on clear-sky

data to obtain $\Delta\mathrm{CRE}$ (as mentioned in the previous section). BESM features G = 8.62 W m^{-2}, λ = -1.45 W m^{-2} K^{-1}, $\Delta\mathrm{CRE}$ = -0.13 W m^{-2} K^{-1}, and ECS = 2.96 K.

The parameters G, λ, $\Delta\mathrm{CRE}$ and ECS computed for all models are shown in Table 3. The climate sensitivities of 26 CMIP5 coupled models (including BESM-OA2.5) were assessed as it was performed by Andrews et al. (2012) for 15 CMIP5 coupled models. In the present work, we included the following models: ACCESS1-0, ACCESS1-3, bcc-csm1-1, BESM-OA2.5, BNU-ESM, CCSM4, FGOALS-g2, FGOALS-s2, GISS-E2-H, GISS-E2-R, e inmcm4. For the 15 same models, we found similar results to those of Andrews et al. (2012), which range between 2.07 to 4.74 K. The possibly small differences we attribute to the interpolation of the data as detailed in previous section. G and λ vary from 5.01 to 8.95 W m^{-2} and from -1.66 to -0.60 W m^{-2}K^{-1}, respectively. Inter-model spread in G among the models are due to differences in the radiative codes used, as well as the rapid adjustment processes of the troposphere and surface (Collins et al., 2006; Gregory and Webb, 2008; Andrews and Forster, 2008). The spread in the ECS is more influenced by λ than G (Figure 2), as was also suggested by Andrews et al. (2012). The correlation coefficient between ECS and λ is -0.82, which is significant at 1% of confidence interval (Figure 2b). On the other hand, the correlation between ECS and G is -0.01, witch is not statistically significant (Figure 2a). Thus, the ratio of climate restoration (associated with λ) better explains the dispersion in ECS than the initial radiative imbalance triggered by the CO_2 increase (related to G). Despite BESM presenting one of the highest G among all the CMIP5 models, it shows a response to doubling CO_2, which is inside the warming range of 3.30$\pm$0.76 K presented by the models of the ensemble.

$\Delta\mathrm{CRE}$ for BESM is -0.13, while CMIP5 models have $\Delta\mathrm{CRE}$ varying from -0.50 to 0.70 W m^{-2} K^{-1}. This term does not consider the masking effects of clouds as the $\Delta\mathrm{CRE}_a$ estimated by the radiative kernel method (Eq. 5). Therefore, $\Delta\mathrm{CRE}$ cannot be interpreted as a change in the cloud properties alone.

4.2 Climate Feedbacks estimated by Radiative Kernel method

Figure 3 shows the global-mean feedbacks for lapse-rate, water vapor, lapse-rate plus water-vapor, albedo, and cloud (SW, LW, and total) for each CMIP5 model. Both radiative kernels are used to test whether the results are sensitive to the particular choice of radiative kernel, and whether inter-model differences are greater than the distribution of the radiatively active constituents of the base model. It is worth clarifying that positive/negative values of feedbacks contribute to the amplification/damping of global warming. The strongest positive feedback (Figure 3) is due to the water vapor (mean value: 1.39 W m^{-2}K^{-1}), followed by clouds (mean value: 0.96 W m^{-2}K^{-1}), and surface albedo (mean value: 0.32 W m^{-2}K^{-1}). The Planck feedback global-mean is negative with an average of -3.60 W m^{-2}K^{-1} (not shown in Figure 3) followed by lapse-rate feedback with -0.77 W m^{-2}K^{-1}.

For all models in Figure 4, there is an almost constant Planck feedback about -4 W m^{-2} K^{-1} from 90°S to 60°N, with a notable increased ensemble standard deviation in the subantarctic latitude (around 60°S). The exception is in the Arctic region where mean value reaches -10 W m^{-2} K^{-1} with almost the same increased standard deviation. BESM in the subantarctic and Arctic latitudes presented one of the lowest values for Planck feedback, revealing that BESM has a stronger vertically homogeneous warming among the CMIP5 models. Furthermore, for those same region BESM showed greater lapse-rate feedback, corroborating that BESM does not have a higher contrast between surface and upper troposphere temperatures as other models.

As described in Soden et al. (2008), both lapse-rate and water vapor feedbacks partially compensate each other. The stronger increase in upper troposphere temperature than near-surface temperature in all models (shown in Figure 4) results in a negative lapse-rate feedback in the Tropics. On the other hand, the high-latitude warming is more close to the surface, which reflect in a positive lapse-rate feedback. Considering the Clausius-Clapeyron relation, the upper troposphere with an increased temperature could allow more water vapor concentration, leading to a positive water vapor feedback. The opposite is also true, e.g. positive lapse-rate feedback could exist as a result of a lower warming and humidity at the upper troposphere than near the surface, which can be associated with a negative water vapor feedback. However, recently Po-Chedley et al. (2018) showed that the correlation between lapse-rate and water vapor feedbacks is more related to the patter of surface warming than the covariation of the local tropical lapse-rate and water vapor feedbacks. For water vapor feedback it is observed a greater dispersion in the Tropics, with BESM systematically presenting values below of the ensemble mean for the same latitude band. This behavior extends throughout the Northern Hemisphere.

The albedo feedback is important in regions where there is a reduction in sea-ice and snow cover near the Polar Regions (Figure 4). The positive signal of the albedo feedback implies that the reduction in albedo corresponds to an increase in both the radiation budget at the TOA (due to the reduction of upward shortwave radiation) and temperature near the surface. The albedo feedback shows a large dispersion among models in northern high latitudes. It is emphasized that not only the albedo feedback contributes to the Arctic Amplification. In fact, as discussed by Pithan and Mauritsen (2014), the albedo feedback is the second main contributor to Arctic Amplification, while the largest contributor is the temperature feedback. The explanation for the importance of temperature feedback during the surface warming, is in the fact that more energy is radiated back to space in low latitudes, compared with the Arctic. BESM shows an albedo feedback greater than the ensemble standard deviation over Southern ocean around 60°S. This same latitude is where Planck and lapse-rate feedbacks are out of models limits for BESM. Also, as a consequence of sea-ice melting, that region experienced a stronger increase in atmosphere temperature comparatively to the ensemble spread. Those negative values are more evident over the Tropical Pacific and North Atlantic oceans.

Regarding cloud feedbacks, most of the inter-model spread arise from the SW component (figures 3 and 4). This dispersion is also noted in the standard deviation and in the limit between minimum and maximum of zonally averaged cloud feedback shown in Figure 4. The SW cloud feedback ranges from -0.28 to 1.40 W $m^{-2}K^{-1}$, while the LW cloud effect ranges from 0.10 to 0.96 W $m^{-2}K^{-1}$. The combined SW and LW cloud effects result in a positive cloud feedback ranging from 0.35 to 1.69 W $m^{-2}K^{-1}$. This result is similar to that found by Soden et al. (2008) for CMIP3 [IPCC AR4, IPCC (2007)] models, where they presented a near neutral and positive cloud feedback. BESM presents positive values of around 0.5 W $m^{-2}K^{-1}$ for both SW and LW cloud feedback, which results in a total cloud feedback of 1.0 W $m^{-2}K^{-1}$ (Figure 3). The highest positive values are in regions with strong albedo feedback (Figure 4).

Overall, BESM lies within the range of CMIP5 models, with global-mean values of 1.24 W $m^{-2}K^{-1}$, 0.95 W $m^{-2}K^{-1}$, 0.27 W $m^{-2}K^{-1}$, -3.57 W $m^{-2}K^{-1}$ and -0.71 W $m^{-2}K^{-1}$ for water vapor, cloud, albedo feedbacks, Planck and lapse-rate feedbacks, respectively. However, differences between BESM and the other models are found in the high latitudes, where BESM exhibit lapse-rate and humidity feedbacks marginally out of range of values set by the CMIP5 multi-model ensemble (Figure 4). It is also evident from figures 4 and 5 that BESM is an outlier for the cloud feedbacks. This is due to a strong

shortwave component response over both the Arctic and the Southern Ocean near Antarctica. Considering the SW CRE [as described by Cess et al. (1989)] and the individual components of feedback cloud mask, we can note that those higher values in cloud feedback are mainly consequences of the sum of SW CRE and the effect of cloud masking for albedo feedback $[-(\lambda_a - \lambda_{ac})]$, as shown in Figure 6. For Arctic region, the major contributor for BESM be an outlier is the SW CRE, while for over the ocean near the Antarctic is the albedo feedback cloud mask. In this latter, since the radiative kernel for both all- and clear-sky are the same throughout the models, the difference among them is the albedo change $[\Delta a/\Delta\bar{\bar{T}}_{as}(K_a - K_a^{cs})]$. Over the both regions (Arctic and near Antarctic), an increase in cloud fraction above 850 hPa and a decrease below that level for BESM is observed, which means a low-level clouds upward shifting . Moreover, the increase in cloud cover above 850 hP is stronger than the reduction below (Figure 7a). As consequence, a negative SW CRE change is present in those regions (but not stronger for BESM comparatively to other models), that is the response to the increase in sun shading (Figure 7b). However, the SW cooling is smaller than the heating provided by LW radiation, as presented in the net effect (Figure 7d). The net radiation heating change is more intense around 60°S, that can be related to the more intense surface albedo change, as well as the low-cloud lifting. Despite of the lost of SW energy at surface (related to the increased sun shading), which results in a SW cloud radiative effect negative, it is overcome by the albedo feedback cloud mask, that contribute to a cloud feedback positive over those two regions.

4.3 Changes in temperature, atmospheric circulation and precipitation

Figure 8 shows the annual mean for surface temperature change between the abrupt4xCO2 and piControl scenarios for the ensemble of 25 CMIP5 models and BESM. It is clearly seen in Figure 8 that despite the generalized increase of the air temperature over most of the globe in both panels, BESM shows a generally lower temperature increase, principally over the continental areas. The CMIP5 ensemble shows a mean continental temperature increase of 6.78 K, while BESM shows 5.57 K. Notwithstanding, the spatial pattern of temperature increase is similar, as measured by the spatial inner product (as described in the previous section) between the two upper panels in Figure 8, which results in the value of 0.96 (values near 1 mean that both variables have similar spatial pattern, whereas values near 0 mean that there are few spatial correspondences between variables). One point of interest of the scientific community is the relative low temperature increase over the subpolar North Atlantic, also refered as warming hole (Drijfhout et al., 2012). In the CMIP5 ensemble mean, the North Atlantic does not show a decrease of temperature, but it is the region with the smallest temperature increase globally; while BESM shows an area of temperature decrease in this region. Such a decrease is also present in other 6 analyzed models (CSIRO-Mk3-6-0, FGOALS-s2, GFDL-ESM2G, GFDL-ESM2M, GISS-E2-R, and inmcm4). This results are consistent with Drijfhout et al. (2012), who showed that both observations and CMIP5 models present maximum cooling in the center of the subpolar gyre. Those authors argue that there are evidences that both subpolar gyre and AMOC adjust in concert with different time lags.

The regions with the largest temperature increase in the abrupt4xCO2 scenario are the Polar Regions, mainly over the North Pole. The equatorial Pacific shows an increase in temperature in the abrupt4xCO2 scenario when compared with the piControl, both in the CMIP5 ensemble and BESM. Such changes in the Pacific mean state is in line with the IPCC-AR5, in which it is shown that the Pacific Ocean becomes warmer near the equator compared to the subtropics in the CMIP5 projections (Liu

et al., 2005; Gastineau and Soden, 2009; Cai et al., 2015). The scatter plot of global average of abrupt4xCO2 versus piControl presented in Figure 8 is an additional information that helps to understand the models dispersion around the mean value. Even though there is a predominance of models in either quadrants 1 or 3 (top-right and bottom-left, respectively), it is not possible to note a linear relationship. It means that models with warmer/cooler mean climates in the piControl runs aparently does not present a corresponding warmer/cooler climate for the abrupt4xCO2 experiments.

Figure 9 shows the precipitation changes between abrupt4xCO2 and piControl scenarios for multi-model ensemble and BESM. The results are approximately similar to Held and Soden (2006), with wet regions becoming wetter (near-equatorial and subpolar regions) and dry regions becoming drier (centered around 30° in both hemispheres). The precipitation pattern in the CMIP5 ensemble has increased precipitation over the equatorial Pacific, which can be related to the equatorial Pacific warming pattern shown in the temperature change (Figure 8). Also, the CMIP5 ensemble shows a decrease in precipitation in northern South America. BESM precipitation pattern is similar to the spatial patterns in the CMIP5 ensemble, yet with some notable discrepancies. For example, the decrease in precipitation over the South Pacific shown in the CMIP5 ensemble plot is extended into the Indonesian region in BESM. It is also worth noting in the BESM simulation that the South Pacific convergence zone (SPCZ) shifts southward in the abrupt4xCO2, compared to piControl. Over South America, the precipitation change pattern is similar to that which occurs during El Niño years (Kayano et al., 1988; Marengo and Hastenrath, 1993; Grimm and Tedeschi, 2009), with increased precipitation over southeastern South America and decreased precipitation over northern/northeastern South America, in both the multi-model ensemble and BESM. The scatter plot in Figure 9 suggests a linear relationship between experiments, meaning that models that have a larger (smaller) global average precipitation in piControl scenario show a larger (smaller) precipitation in abrupt4xCO2 scenario. In the scatter plot of Figure 9, BESM has value near the center, which means that it presents global averaged precipitation values similar to the average of all the models used in the ensemble.

Figure 10 depicts the scatter plot of ECS versus the change in precipitation between Abrupt4xCO2 and piControl (ΔPr), for all models considered. It is worth noting that all the models present increased global-mean precipitation for the quadrupling of atmospheric CO_2 with piControl pre-industrial CO_2 concentrations (positive values in y-axis in Figure 10). The apparent linear relationship between differences (abrupt4xCO2 minus piControl) in global-mean precipitation and ECS is also evident in Figure 10, in which warmest models tend to have highest changes in precipitation. The slope of the linear regression is 2.5% of precipitation change per K, which is close to that found by Held and Soden (2006).This slope is much inferior to that expected for Clausius-Clapeyron relation, which is about 6,5% of precipitation chang per K. In fact, precipitation increasing is not governed by the availability of moisture but by the surface and tropospheric energy balance, including in this process the surface radiative heating, surface latent heat flux and radiative cooling of troposphere (Allen and Ingram, 2002).

MRI-CGCM3, ACCESS1-0, and HadGEM2-ES show greater deviation from the linear fit shown in Figure 10. Also, BESM is marginally out of the residual standard error interval, with 9.5% increased precipitation (the error limit is 9.2%). ACCESS1-0 and HadGEM2-ES use the same atmospheric model (Bi et al., 2013; Dix et al., 2013), which could explain the lower increase in precipitation in both coupled models.

As in the case of temperature and precipitation changes, we are also interested in understanding the alteration in the BESM atmospheric circulation (compared to other models) considering a quadrupling of CO_2 concentration. The sea level pressure (SLP) response patterns shown in Figure 11 depict a poleward shift of the subtropical high pressure cells for both the CMIP5 ensemble and BESM. Furthermore, when the models are subjected to the increase of atmospheric CO_2 concentration, a decrease in SLP over the Polar regions is evident. This SLP decrease over the Polar regions and the increase in mid-latitudes indicate a positive trend of Arctic Oscillation (AO) and Antarctic Oscillation (AAO) episodes, which have already been reported in the studies of Fyfe et al. (1999), Cai et al. (2003), Miller et al. (2006). It is also interesting to note the statistically significant SLP decrease (increase) over the eastern (western) Pacific, a pattern that might be indicative of an ENSO-like pattern in scenarios with increased CO_2 concentration. This pattern is coherent with those depicted in Figure 8 for SST changes in a 4xCO_2 scenario.

Results for piControl scenario (contours in Figure 12) show that the Southern Hemisphere subtropical jet, depicted by the core of maximum eastward zonal wind, is localized around 35°S, 200-150 hPa, in both the CMIP5 ensemble and BESM. We note that regions with the strongest positive values (anomalous eastward wind) in all levels show a southward displacement in both panels of Figure 12 (BESM and the CMIP5 ensemble). This is consistent with the poleward displacement of high SLP center shown in Figure 11. Also, as the high-pressure centers experienced a poleward shift, the pressure gradients are intensified in subpolar areas, and consequently increased near-surface wind velocity is a result, following the geostrophic approximation $[u \approx -(1/f\rho)(\partial p/\partial y)]$, where f is the Coriolis parameter and ρ is the air density.

Figure 13 shows the average 5°N – 5°S (Walker circulation) differences between abrupt4xCO2 and piControl for omega (shades) and zonal wind and vertical velocity (vectors). According to the pattern of omega in piControl (contours), the multi-model ensemble and BESM show subsidence over an extensive area in the Pacific (150°E – 90°W), which intensity is reduced in the abrupt4xCO2 simulation, as indicated in Figure 13 (blue). This is coherent with near-surface temperature patterns (Figure 8), which show an equatorial warming pattern in the mean state (e.g. during El Niño years a weakening of the Walker circulation occurs). Furthermore, there are positive values in the difference between the two scenarios over South America (around 75°W), consistent with the decrease of precipitation in tropical South America, in both BESM and the CMIP5 ensemble (Figure 9).

5 Conclusions

piControl and abrupt4xCO2 scenarios for 25 CMIP5 models have been contrasted with those generated by the BESM-OA2.5 model, based on their climate sensitivity parameters such as the Equilibrium Climate Sensitivity (ECS) and climate feedbacks. Also, the changes in the temperature, atmospheric circulation and precipitation patterns were investigated.

Applying the linear regression method (Gregory et al., 2004), we obtain ECS for the 25 CMIP5 models analyzed ranging from 2.07 to 4.74 K, with BESM showing 2.96 K, close to the ensemble mean value (3.30 $\pm$ 0.76). BESM has one of the biggest radiative forcing (G) with 8,62 W m^{-2}K, which is related to the radiative code transference and the rapid adjustment process (Collins et al., 2006; Gregory and Webb, 2008; Andrews and Forster, 2008). Both G and the climate sensitivity (λ)

define the ECS with this method, however, only λ presents a significant correlation with ECS, corroborating with Andrews et al. (2012) results.

To go further in the analysis, the radiative kernel method is used to separate the climate feedback into Planck, lapse-rate, water vapor, albedo and cloud feedbacks. Two regions presented considerable standard deviation for Plank, lapse-rate and albedo: the Arctic region and over the ocean near the Antarctic. Over those regions, BESM-OA2.5 also shows cloud feedback values larger than the zonal mean plus standard deviation for the analyzed models, reaching near 3 W $m^{-2}K^{-1}$ while the zonal mean is around 0 W $m^{-2}K^{-1}$. For BESM-OA2.5 was observed a shift upward of the low-cloud cover and an increase in cloud cover between 850 and 700 hPa, what is responsible for a sun shading at surface, increasing the outgoing SW radiation at the TOA. Moreover, BESM-OA2.5 presented a greater albedo change than other models, specially in the subantarctic area. Despite of the lost of SW energy at surface, which results in a negative SW cloud radiative effect, it is overcome by the albedo feedback cloud mask, that contribute to a positive cloud feedback over those regions.

Atmospheric circulation patterns in BESM-OA2.5 are similar to patterns in the multi-model ensemble and in other studies regarding near-surface temperature (IPCC, 2007, 2013). For precipitation, the thermodynamic component evidences the well-known 'wet-gets-wetter' and 'dry-gets-drier' pattern of precipitation changes (Held and Soden, 2006). BESM-OA2.5 along with the CMIP5 ensemble have consistent weakening of Walker circulation, principally in the Pacific and over northern South America, which has been reported in previous studies (Collins et al., 2010; DiNezio et al., 2012; Huang and Xie, 2015; Cai et al., 2015). Regarding SLP, both BESM and the CMIP5 ensemble indicate a poleward displacement of the subtropical high pressure systems, as shown in other studies (Fyfe et al., 1999; Cai et al., 2003; Miller et al., 2006). In line with such displacement, the subtropical jet is also shifted polewards, and it is more evident in the Southern Hemisphere.

BESM-OA2.5 is an additional climate model with ability of reproduce changes that are physically understood in order to study the global climate system. In this sense, the BESM results contributed to better understand the inter-model spread in cloud feedback. Furthermore, BESM is under development in order to overcome the present extra-tropical and tropical climate simulation deficiencies, as reported in Casagrande et al. (2016) and Veiga et al. (2018), respectively.

Code and data availability

The BESM-OA2.5 source code is freely available after signature of a license agreement. Please contact Paulo Nobre to obtain the source code and data of BESM-OA2.5.

Competing interests. The authors declare that they have no conflict of interest.

Acknowledgements. This work is supported by Sao Paulo Research Foundation (FAPESP, 2009/50528-6, 2014/50848-9 and 2018/06204-0), National Coordination for High Level Education and Training (CAPES, Grant 16/2014), CAPES/National Water Agency (CAPES/ANA,

88887.115872/2015-01), Brazilian National Council for Scientific and Technological Development (CNPq, 490237/2011-8 and 302218/2016-5), the Brazilian Research Network on Global Climate Change (FINEP/Rede Clima, Grant 01.13.0353-00), National Institute for Science and Technology on Climate Change (INCT-MC 573797/2008-0), and INCT-MC Phase 2 funded by CNPq (Grant 465501/2014-1).

References

Allen, M. R. and Ingram, W. J.: Constraints on future changes in climate and the hydrologic cycle, Nature, 419, 224–232, https://doi.org/10.1038/nature01092, 2002.

Alpert, J. C., Kanamitsu, M., Caplan, P. M., Sela, J. G., White, G. H., and Kalnay, E.: Mountain induced gravity wave drag parameterization in the NMC medium-range forecast model, pp. 726–733, Amer. Metero. Soc., 1988.

Amaya, D. J., DeFlorio, M. J., Miller, A. J., and Xie, S.-P.: WES feedback and the Atlantic Meridional Mode: observations and CMIP5 comparisons, Climate Dynamics, 49, 1665–1679, https://doi.org/10.1007/s00382-016-3411-1, 2017.

Andrews, T. and Forster, P. M.: CO_2 forcing induces semi-direct effects with consequences for climate feedback interpretations, Geophysical Research Letters, 35, https://doi.org/10.1029/2007GL032273, 2008.

Andrews, T., Gregory, J. M., Webb, M. J., and Taylor, K. E.: Forcing, feedbacks and climate sensitivity in CMIP5 coupled atmosphere-ocean climate models, Geophysical Research Letters, 39, n/a–n/a, https://doi.org/10.1029/2012GL051607, 2012.

Arrhenius, S.: On the influence of carbonic acid in the air upon the temperature of the ground., vol. 41, 1896.

Arya, S. P.: Introduction to Micrometeorology, Academic Press, 1988.

Bi, D., Dix, M., Marsland, S., O'Farrell, S., Rashid, H., Uotila, P., Hirst, T., Kowalczyk, E., Golebiewski, M., Sullivan, A., Yan, H., Hannah, N., Franklin, C., Sun, Z., Vohralik, P., Watterson, I., Zhou, X., Fiedler, R., Collier, M., Ma, Y., Noonan, J., Stevens, L., Uhe, P., Zhu, H., Griffies, S., Hill, R., Harris, C., and Puri, K.: The ACCESS Coupled Model: Description, Control Climate and Evaluation, Australian Meteorological and Oceanographic Journal, 63, 41–64, 2013.

Bony, S., Colman, R., Kattsov, V. M., Allan, R. P., Bretherton, C. S., Dufresne, J. L., Hall, A., Hallegatte, S., Holland, M. M., Ingram, W., Randall, D. a., Soden, B. J., Tselioudis, G., and Webb, M. J.: How well do we understand and evaluate climate change feedback processes?, Journal of Climate, 19, 3445–3482, https://doi.org/10.1175/JCLI3819.1, 2006.

Businger, J. A., Wyngaard, J. C., Izumi, Y., and Bradley, E. F.: Flux-Profile Relationships in the Atmospheric Surface Layer, Journal of the Atmospheric Sciences, 28, 181–189, https://doi.org/10.1175/1520-0469(1971)028<0181:FPRITA>2.0.CO;2, 1971.

Cai, W., Whetton, P. H., and Karoly, D. J.: The Response of the Antarctic Oscillation to Increasing and Stabilized Atmospheric CO_2, Journal of Climate, 16, 1525–1538, https://doi.org/10.1175/1520-0442-16.10.1525, 2003.

Cai, W., Santoso, A., Wang, G., Yeh, S.-W., An, S.-I., Cobb, K. M., Collins, M., Guilyardi, E., Jin, F.-F., Kug, J.-S., Lengaigne, M., McPhaden, M. J., Takahashi, K., Timmermann, A., Vecchi, G., Watanabe, M., and Wu, L.: ENSO and greenhouse warming, Nature Climate Change, 5, 849–859, https://doi.org/10.1038/nclimate2743, 2015.

Caldwell, P. M., Zelinka, M. D., Taylor, K. E., and Marvel, K.: Quantifying the Sources of Intermodel Spread in Equilibrium Climate Sensitivity, Journal of Climate, 29, 513–524, https://doi.org/10.1175/JCLI-D-15-0352.1, 2016.

Callendar, G.: The Artificial Production of Carbon Dioxide, Quarterly Journal of the Royal Meteorological Society, 64, 223–240, https://doi.org/10.1002/qj.49706427503, 1938.

Casagrande, F., Nobre, P., de Souza, R. B., Marquez, A. L., Tourigny, E., Capistrano, V., and Mello, R. L.: Arctic Sea Ice: Decadal Simulations and Future Scenarios Using BESM-OA, Atmospheric and Climate Sciences, 06, 351–366, https://doi.org/10.4236/acs.2016.62029, 2016.

Cess, R. D., Potter, G. L., Blanchet, J. P., Boer, G. J., Ghan, S. J., Kiehl, J. T., Le Treut, H., Li, Z.-X., Liang, X.-Z., Mitchell, J. F. B., Morcrette, J.-J., Randall, D. A., Riches, M. R., Roeckner, E., Schlese, U., Slingo, A., Taylor, K. E., Washington, W. M., Wetherald, R. T., and Yagai, I.: Interpretation of Cloud-Climate Feedback as Produced by 14 Atmospheric General Circulation Models, Science, 245, 513–516, https://doi.org/10.1126/science.245.4917.513, 1989.

Cess, R. D., Potter, G. L., Blanchet, J. P., Boer, G. J., and Del Genio, a. D.: Intercomparison and interpretation of climate feedback processes in 19 atmospheric general circulation models, Journal of Geophysical Research, 95, 16 601–16 615, https://doi.org/10.1029/JD095iD10p16601, 1990.

Collins, M., An, S.-I., Cai, W., Ganachaud, A., Guilyardi, E., Jin, F.-F., Jochum, M., Lengaigne, M., Power, S., Timmermann, A., Vecchi, G., and Wittenberg, A.: The impact of global warming on the tropical Pacific Ocean and El Niño, Nature Geoscience, 3, 391–397, https://doi.org/10.1038/ngeo868, 2010.

Collins, W. D., Ramaswamy, V., Schwarzkopf, M. D., Sun, Y., Portmann, R. W., Fu, Q., Casanova, S. E. B., Dufresne, J.-L., Fillmore, D. W., Forster, P. M. D., Galin, V. Y., Gohar, L. K., Ingram, W. J., Kratz, D. P., Lefebvre, M.-P., Li, J., Marquet, P., Oinas, V., Tsushima, Y., Uchiyama, T., and Zhong, W. Y.: Radiative forcing by well-mixed greenhouse gases: Estimates from climate models in the Intergovernmental Panel on Climate Change (IPCC) Fourth Assessment Report (AR4), Journal of Geophysical Research, 111, https://doi.org/10.1029/2005JD006713, 2006.

Cubasch, U. and Cess, R. D.: Processes and modeling. Climate Change: The IPCC Scientific Assessment, Cambridge University Press, 1990.

DiNezio, P. N., Kirtman, B. P., Clement, A. C., Lee, S.-K., Vecchi, G. A., and Wittenberg, A.: Mean Climate Controls on the Simulated Response of ENSO to Increasing Greenhouse Gases, Journal of Climate, 25, 7399–7420, https://doi.org/10.1175/JCLI-D-11-00494.1, 2012.

Dix, M., Vohralik, P., Bi, D., Rashid, H., Marsland, S., O'Farrell, S., Uotila, P., Hirst, T., Kowalczyk, E., Sullivan, A., Yan, H., Franklin, C., Sun, Z., Watterson, I., Collier, M., Noonan, J., Rotstayn, L., Stevens, S., Uhe, P., and Puri, K.: The ACCESS coupled model: description, control climate and evaluation, Australian Meteorological and Oceanographic Journal, 63, 83–99, 2013.

Drijfhout, S., van Oldenborgh, G. J., and Cimatoribus, A.: Is a Decline of AMOC Causing the Warming Hole above the North Atlantic in Observed and Modeled Warming Patterns?, Journal of Climate, 25, 8373–8379, https://doi.org/10.1175/JCLI-D-12-00490.1, 2012.

Dufresne, J.-L. and Bony, S.: An Assessment of the Primary Sources of Spread of Global Warming Estimates from Coupled Atmosphere–Ocean Models, Journal of Climate, 21, 5135–5144, https://doi.org/10.1175/2008JCLI2239.1, 2008.

Eyring, V., Bony, S., Meehl, G. A., Senior, C. A., Stevens, B., Stouffer, R. J., and Taylor, K. E.: Overview of the Coupled Model Intercomparison Project Phase 6 (CMIP6) experimental design and organization, Geoscientific Model Development, 9, 1937–1958, https://doi.org/10.5194/gmd-9-1937-2016, 2016.

Ferrier, B. S., Jin, Y., Lin, Y., Black, T., Rogers, E., and DiMego, G.: Implementation of a new grid-scale cloud and precipitation scheme in the NCEP Eta Model, pp. 280–283, Amer. Meteor. Soc., 2002.

Figueroa, S. N., Kubota, P. Y., Grell, G., Morrison, H., Bonatti, J. P., Barros, S., Fernandez, J. P., Ramirez, E., Siqueira, L., Satyamurti, P., Luzia, G., da Silva, J., da Silva, J., Pendharkar, J., Capistrano, V. B., Alvin, D., Enore, D., Denis, F., Rozante, J. R., Cavalcanti, I., Barbosa, H., Mendes, C., and Tarassova, T.: The Brazilian Global Atmospheric Model (BAM). Part I: Performance for Tropical Rainfall forecasting and sensitivity to convective schemes and horizontal resolutions, Weather and Forecasting, 31, 1547–1572, https://doi.org/10.1175/WAF-D-16-0062.1, 2016.

Foley, J. a., Prentice, I. C., Ramankutty, N., Levis, S., Pollard, D., Sitch, S., and Haxeltine, a.: An integrated biosphere model of land surface processes, terrestrial carbon balance, and vegetation dynamics, vol. 10, 1996.

Fyfe, J. C., Boer, G. J., and Flato, G. M.: The Arctic and Antarctic oscillations and their projected changes under global warming, Geophysical Research Letters, 26, 1601–1604, https://doi.org/10.1029/1999GL900317, 1999.

Gastineau, G. and Soden, B. J.: Model projected changes of extreme wind events in response to global warming, Geophysical Research Letters, 36, https://doi.org/10.1029/2009GL037500, 2009.

Good, P., Andrews, T., Chadwick, R., Dufresne, J.-L., Gregory, J. M., Lowe, J. A., Schaller, N., and Shiogama, H.: nonlinMIP contribution to CMIP6: model intercomparison project for non-linear mechanisms: physical basis, experimental design and analysis principles (v1.0), Geoscientific Model Development, 9, 4019–4028, https://doi.org/10.5194/gmd-9-4019-2016, 2016.

Gregory, J. and Webb, M.: Tropospheric Adjustment Induces a Cloud Component in CO_2 Forcing, Journal of Climate, 21, 58–71, https://doi.org/10.1175/2007JCLI1834.1, 2008.

Gregory, J. M., Ingram, W. J., Palmer, M. A., Jones, G. S., Stott, P. A., Thorpe, R. B., Lowe, J. A., Jonhs, T. C., and Williams, K. D.: A new method for diagnosing radiative forcing and climate sensitivity, Geophysical Research Letters, 31, L03 205, https://doi.org/10.1029/2003GL018747, 2004.

Grell, G. A. and Dévényi, D.: A generalized approach to parameterizing convection combining ensemble and data assimilation techniques: PARAMETERIZING CONVECTION COMBINING ENSEMBLE AND DATA ASSIMILATION TECHNIQUES, 29, 38–1–38–4, https://doi.org/10.1029/2002GL015311, http://doi.wiley.com/10.1029/2002GL015311, 2002.

Griffies, S. M., Harrison, M. J., Pacanowski, Ronald, C., and Rosati, A.: A Technical Guide to MOM4, GFDL Ocean Group Technical Report No. 5, NOAA/Geophysical Fluid Dynamics Laboratory, p. Available online atwww.gfdl.noaa.gov, 2004.

Grimm, A. M. and Tedeschi, R. G.: ENSO and Extreme Rainfall Events in South America, Journal of Climate, 22, 1589–1609, https://doi.org/10.1175/2008JCLI2429.1, 2009.

Harshvardhan, Davies, R., Randall, D. A., and Corsetti, T. G.: A fast radiation parameterization for atmospheric circulation models, Journal of Geophysical Research, 92, 1009, https://doi.org/10.1029/JD092iD01p01009, 1987.

Held, I. M. and Soden, B. J.: Robust Responses of the Hydrological Cycle to Global Warming, Journal of Climate, 19, 5686–5699, https://doi.org/10.1175/JCLI3990.1, 2006.

Holtslag, a. a. M. and Boville, B. a.: Local versus nonlocal boundary-layer diffusion in a global climate model, vol. 6, 1993.

Huang, P. and Xie, S.-P.: Mechanisms of change in ENSO-induced tropical Pacific rainfall variability in a warming climate, Nature Geoscience, 8, 922–926, https://doi.org/10.1038/ngeo2571, 2015.

Iacono, M. J., Delamere, J. S., Mlawer, E. J., Shephard, M. W., Clough, S. A., and Collins, W. D.: Radiative forcing by long-lived greenhouse gases: Calculations with the AER radiative transfer models, Journal of Geophysical Research, 113, https://doi.org/10.1029/2008JD009944, 2008.

IPCC: Climate change 2007: the physical science basis; contribution of Working Group I to the Fourth Assessment Report of the Intergovernmental Panel on Climate Change, 2007.

IPCC: Climate change 2013: the physical science basis; Working Group I contribution to the Fifth Assessment Report of the Intergovernmental Panel on Climate Change, 2013.

Jiménez, P. a., Dudhia, J., González-Rouco, J. F., Navarro, J., Montávez, J. P., and García-Bustamante, E.: A Revised Scheme for the WRF Surface Layer Formulation, Monthly Weather Review, 140, 898–918, https://doi.org/10.1175/MWR-D-11-00056.1, 2012.

Jonko, A. K., Shell, K. M., Sanderson, B. M., and Danabasoglu, G.: Climate Feedbacks in CCSM3 under Changing CO_2 Forcing. Part II: Variation of Climate Feedbacks and Sensitivity with Forcing, Journal of Climate, 26, 2784–2795, https://doi.org/10.1175/JCLI-D-12-00479.1, 2013.

Kanamitsu, M., Ebisuzaki, W., Woollen, J., Yang, S.-K., Hnilo, J. J., Fiorino, M., and Potter, G. L.: NCEP–DOE AMIP-II Reanalysis (R-2), Bulletin of the American Meteorological Society, 83, 1631–1643, https://doi.org/10.1175/BAMS-83-11-1631, 2002.

Kaplan, L. D.: The Influence of Carbon Dioxide Variations on the Atmospheric Heat Balance, Tellus, 12, 204–208, https://doi.org/10.1111/j.2153-3490.1960.tb01301.x, 1960.

Kayano, M. T., Rao, V. B., and Moura, A. D.: Tropical circulations and the associated rainfall anomalies during two contrasting years, Journal of Climatology, 8, 477–488, https://doi.org/10.1002/joc.3370080504, 1988.

Kubota, P. Y.: Variability of stored energy in the surface and its impact on the definition of the precipitation pattern over South America (Variablidade de energia armazenada na superfície e seu impacto na definição do padrão de precipitação na América do Sul), Ph.D. thesis, National Institute for Space Research (INPE), [Available online at http://mtc-m16d.sid.inpe.br/col/sid.inpe.br/mtc-m19/2012/08.02.02.42/doc/publicacao.pdf], 2012.

Liu, H., Wang, C., Lee, S.-K., and Enfield, D.: Atlantic Warm Pool Variability in the CMIP5 Simulations, Journal of Climate, 26, 5315–5336, https://doi.org/10.1175/JCLI-D-12-00556.1, 2013.

Liu, Z., Vavrus, S., He, F., Wen, N., and Zhong, Y.: Rethinking Tropical Ocean Response to Global Warming: The Enhanced Equatorial Warming*, Journal of Climate, 18, 4684–4700, https://doi.org/10.1175/JCLI3579.1, 2005.

Manabe, S. and Stouffer, R. J.: Sensitivity of a global climate model to an increase of CO2 concentration in the atmosphere, Journal of Geophysical Research, 85, 5529–5554, https://doi.org/10.1029/JC085iC10p05529, 1980.

Manabe, S. and Wetherald, R. T.: Thermal Equilibrium of the Atmosphere with a Given Distribution of Relative Humidity, Journal of the Atmospheric Sciences, 24, 241–259, 1967.

Manabe, S. and Wetherald, R. T.: The Effects of Doubling the CO_2 Concentration on the climate of a General Circulation Model, Journal of the Atmospheric Sciences, 32, 3–15, https://doi.org/10.1175/1520-0469(1975)032<0003:TEODTC>2.0.CO;2, 1975.

Marengo, J. A. and Hastenrath, S.: Case Studies of Extreme Climatic Events in the Amazon Basin, Journal of Climate, 6, 617–627, https://doi.org/10.1175/1520-0442(1993)006<0617:CSOECE>2.0.CO;2, 1993.

Marvel, K. and Bonfils, C.: Identifying external influences on global precipitation, Proceedings of the National Academy of Sciences, 110, 19 301–19 306, https://doi.org/10.1073/pnas.1314382110, http://www.pnas.org/cgi/doi/10.1073/pnas.1314382110, 2013.

Mellor, G. L. and Yamada, T.: Development of a turbulence closure model for geophysical fluid problems, Reviews of Geophysics, 20, 851, https://doi.org/10.1029/RG020i004p00851, 1982.

Miller, R. L., Schmidt, G. A., and Shindell, D. T.: Forced annular variations in the 20th century Intergovernmental Panel on Climate Change Fourth Assessment Report models, Journal of Geophysical Research, 111, https://doi.org/10.1029/2005JD006323, 2006.

Morrison, H., Curry, J. A., and Khvorostyanov, V. I.: A New Double-Moment Microphysics Parameterization for Application in Cloud and Climate Models. Part I: Description, Journal of the Atmospheric Sciences, 62, 1665–1677, https://doi.org/10.1175/JAS3446.1, 2005.

Nobre, P. and Srukla, J.: Variations of Sea Surface Temperature, Wind Stress, and Rainfall over the Tropical Atlantic and South America, Journal of Climate, 9, 2464–2479, https://doi.org/10.1175/1520-0442(1996)009<2464:VOSSTW>2.0.CO;2, 1996.

Nobre, P., Siqueira, L. S. P., de Almeida, R. A. F., Malagutti, M., Giarolla, E., Castelão, G. P., Bottino, M. J., Kubota, P., Figueroa, S. N., Costa, M. C., Baptista, M., Irber, L., and Marcondes, G. G.: Climate Simulation and Change in the Brazilian Climate Model, Journal of Climate, 26, 6716–6732, https://doi.org/10.1175/JCLI-D-12-00580.1, 2013.

Park, S. and Bretherton, C. S.: The University of Washington Shallow Convection and Moist Turbulence Schemes and Their Impact on Climate Simulations with the Community Atmosphere Model, 22, 3449–3469, https://doi.org/10.1175/2008JCLI2557.1, http://journals.ametsoc.org/doi/abs/10.1175/2008JCLI2557.1, 2009.

Pincus, R., Forster, P. M., and Stevens, B.: The Radiative Forcing Model Intercomparison Project (RFMIP): experimental protocol for CMIP6, Geoscientific Model Development, 9, 3447–3460, https://doi.org/10.5194/gmd-9-3447-2016, 2016.

Pithan, F. and Mauritsen, T.: Arctic amplification dominated by temperature feedbacks in contemporary climate models, Nature Geoscience, 7, 181–184, https://doi.org/10.1038/ngeo2071, 2014.

Plass, G. N.: The Carbon Dioxide Theory of Climatic Change, Tellus, 8, 140–154, https://doi.org/10.1111/j.2153-3490.1956.tb01206.x, 1956.

Richter, I., Xie, S.-P., Behera, S. K., Doi, T., and Masumoto, Y.: Equatorial Atlantic variability and its relation to mean state biases in CMIP5, Climate Dynamics, 42, 171–188, https://doi.org/10.1007/s00382-012-1624-5, 2014.

Seager, R., Naik, N., and Vecchi, G. A.: Thermodynamic and Dynamic Mechanisms for Large-Scale Changes in the Hydrological Cycle in Response to Global Warming*, Journal of Climate, 23, 4651–4668, https://doi.org/10.1175/2010JCLI3655.1, http://journals.ametsoc.org/doi/abs/10.1175/2010JCLI3655.1, 2010.

Shell, K. M., Kiehl, J. T., and Shields, C. a.: Using the radiative kernel technique to calculate climate feedbacks in NCAR's Community Atmospheric Model, Journal of Climate, 21, 2269–2282, https://doi.org/10.1175/2007JCLI2044.1, 2008.

Slingo, J. M.: The Development and Verification of A Cloud Prediction Scheme For the ECMWF Model, Quarterly Journal of the Royal Meteorological Society, 113, 899–927, https://doi.org/10.1002/qj.49711347710, 1987.

Soden, B. and Held, I.: An Assessment of Climate Feedbacks in Coupled Ocean – Atmosphere Models, Journal of Climate, 19, 3354–3360, https://doi.org/10.1175/JCLI9028.1, 2006.

Soden, B. J., Broccoli, A. J., and Hemler, R. S.: On the use of cloud forcing to estimate cloud feedback, Journal of Climate, 17, 3661–3665, https://doi.org/10.1175/1520-0442(2004)017<3661:OTUOCF>2.0.CO;2, 2004.

Soden, B. J., Held, I. M., Colman, R., Shell, K. M., Kiehl, J. T., and Shields, C. A.: Quantifying Climate Feedbacks Using Radiative Kernels, Journal of Climate, 21, 3504–3520, https://doi.org/10.1175/2007JCLI2110.1, 2008.

Soden, B. J., Collins, W. D., and Feldman, D. R.: Reducing uncertainties in climate models, Science, 361, 326–327, https://doi.org/10.1126/science.aau1864, http://www.sciencemag.org/lookup/doi/10.1126/science.aau1864, 2018.

Tarasova, T. a. and Fomin, B. a.: The Use of New Parameterizations for Gaseous Absorption in the CLIRAD-SW Solar Radiation Code for Models, Journal of Atmospheric and Oceanic Technology, 24, 1157–1162, https://doi.org/10.1175/JTECH2023.1, 2007.

Taylor, K. E., Stouffer, R. J., and Meehl, G. a.: An overview of CMIP5 and the experiment design, Bulletin of the American Meteorological Society, 93, 485–498, https://doi.org/10.1175/BAMS-D-11-00094.1, 2012.

Tiedtke, M.: The sensitivity of the time mean large-scale flow to cumulus convection in the ECMWF model. Workshop on Convection in Large-Scale Numerical Model, pp. 297–316, ECMWF, 1984.

Veiga, S. F., Nobre, P., Giarolla, E., Capistrano, V., Baptista Jr., M., Marquez, A. L., Figueroa, S. N., Bonatti, J. P., Kubota, P., and Nobre, C. A.: The Brazilian Earth System Model version 2.5: Evaluation of its CMIP5 historical simulation, Geoscientific Model Development Discussions, pp. 1–73, https://doi.org/10.5194/gmd-2018-91, 2018.

Vial, J., Dufresne, J.-L., and Bony, S.: On the interpretation of inter-model spread in CMIP5 climate sensitivity estimates, Climate Dynamics, 41, 3339–3362, https://doi.org/10.1007/s00382-013-1725-9, 2013.

Webster, S., Brown, A. R., Cameron, D. R., and P.Jones, C.: Improvements to the representation of orography in the Met Office Unified Model, 129, 1989–2010, https://doi.org/10.1256/qj.02.133, http://doi.wiley.com/10.1256/qj.02.133, 2003.

Xie, S.-P., Deser, C., Vecchi, G. A., Collins, M., Delworth, T. L., Hall, A., Hawkins, E., Johnson, N. C., Cassou, C., Giannini, A., and Watanabe, M.: Towards predictive understanding of regional climate change, Nature Climate Change, 5, 921–930, https://doi.org/10.1038/nclimate2689, 2015.

Xue, Y., Sellers, P. J., Kinter, J. L., and Shukla, J.: A simplified biosphere model for global climate studies, Journal of Climate, 4, 345–364, 1991.

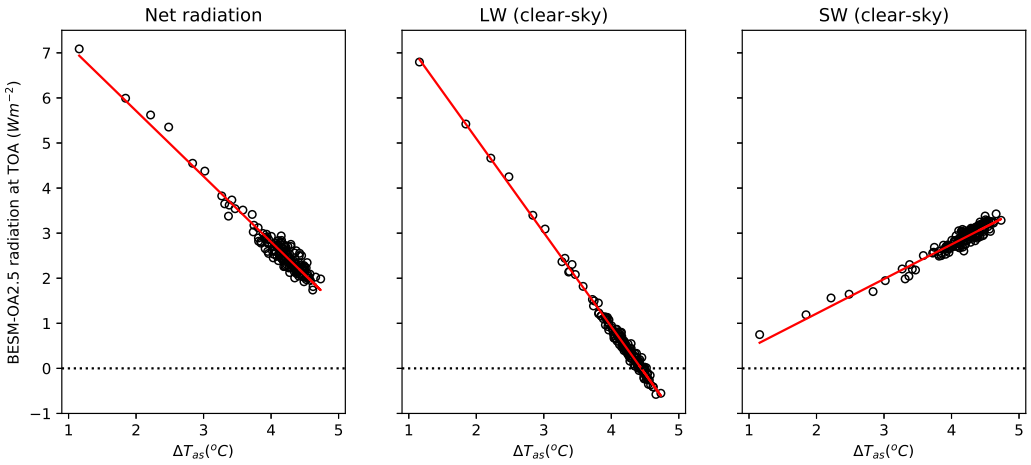

Figure 1. Annual global-mean linear regression between $\Delta\overline{T}_{as}$ and: (a) Net radiation, (b) ΔLW (clear-sky) (c) ΔSW (clear-sky) for BESM-OA2.5

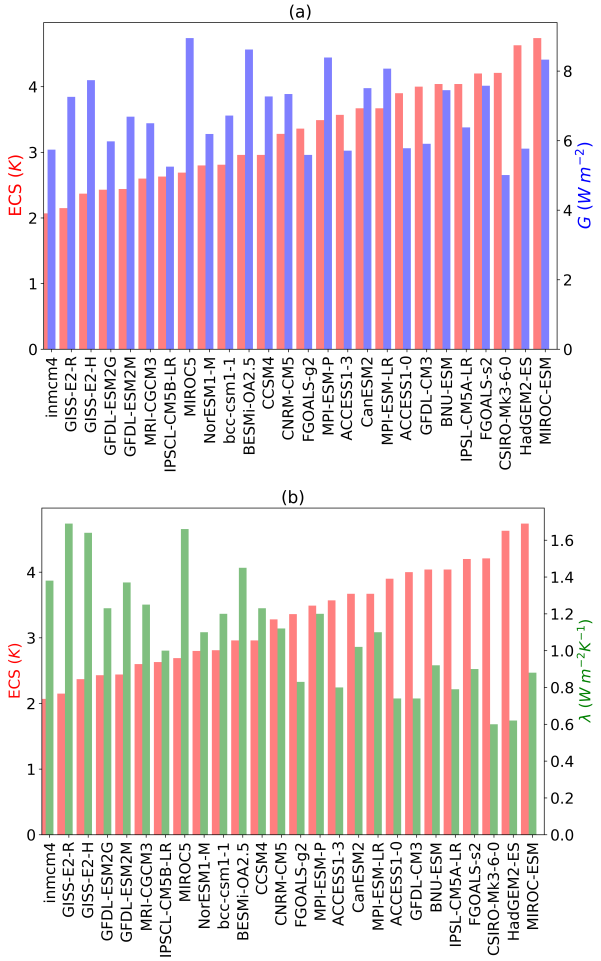

Figure 2. (a) Equilibrium Climate Sensitivity (ECS, in red) and Radiative forcing (G, in blue) values with ECS increasing from left to right; (b) ECS (red) and climate sensitivity (λ, in green) with ECS increasing from left to right.

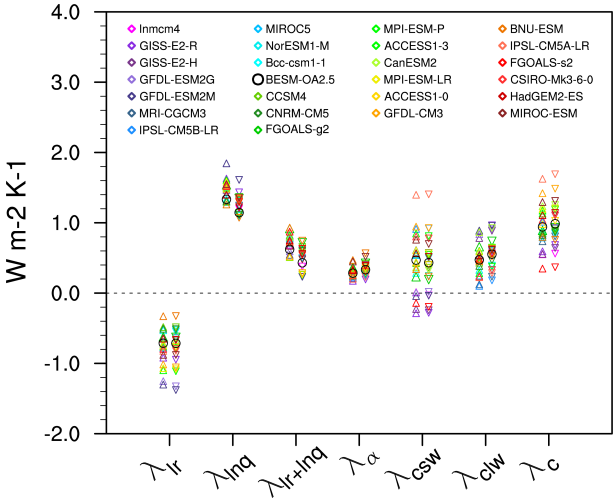

Figure 3. Global-mean feedbacks for 25 CMIP5 models and BESM-OA2.5 (circle). Changes in abrupt4xCO2 relative to piControl are averaged over years 120-150. The triangles mean estimated feedback values using NCAR radiative kernel whereas upside-down triangles mean estimated feedback values using GFDL radiative kernel.

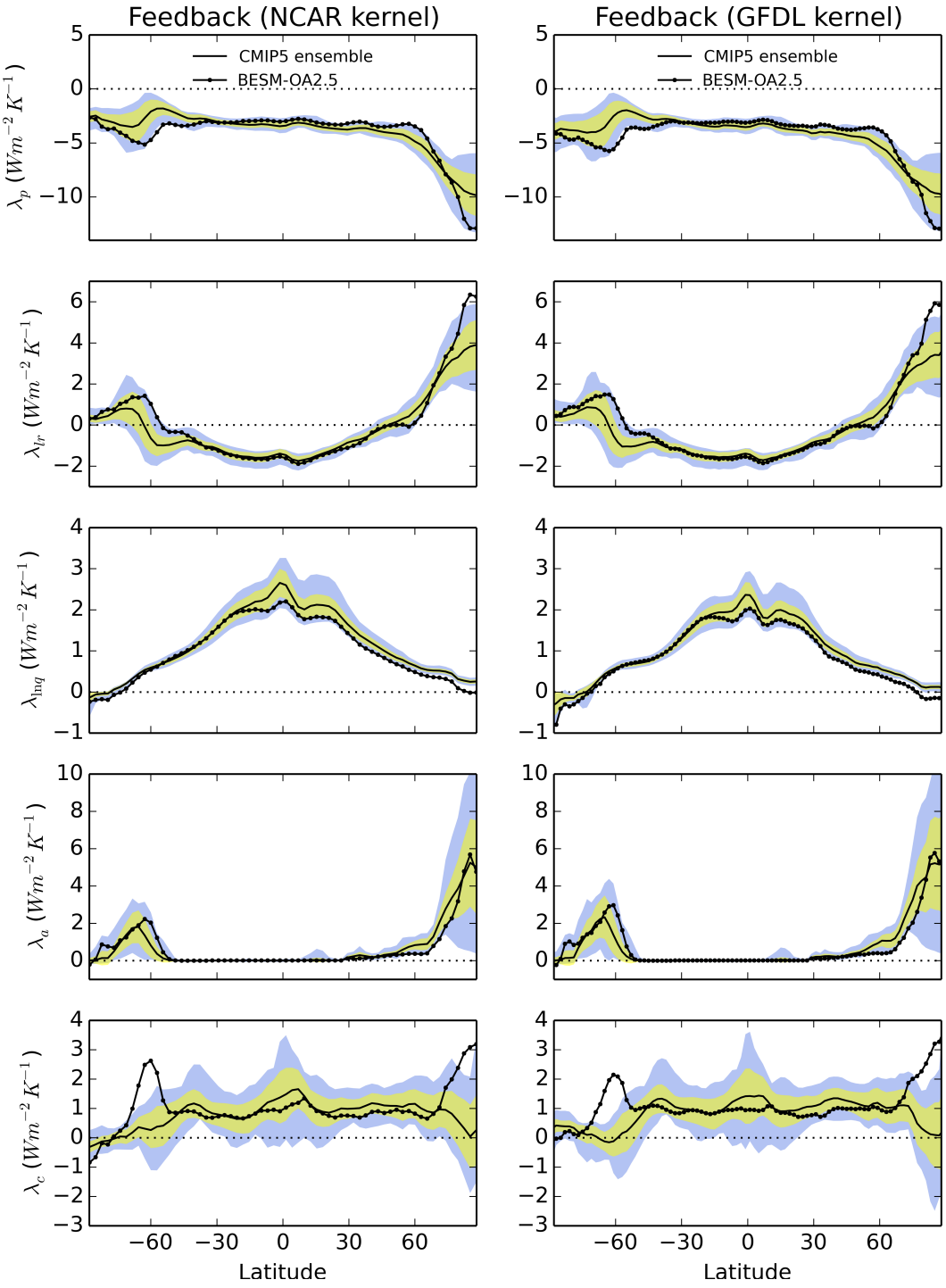

Figure 4. Feedbacks for the CMIP5 multi-model ensemble-mean (solid line) and BESM-OA2.5 (solid line with dots). Inter-model standard deviations for each latitude are in yellow. In blue are the feedback limits based on the maximum and minimum values for each latitude among the models, not including BESM-OA2.5. All feedbacks are based on the averaged over years 120-150.

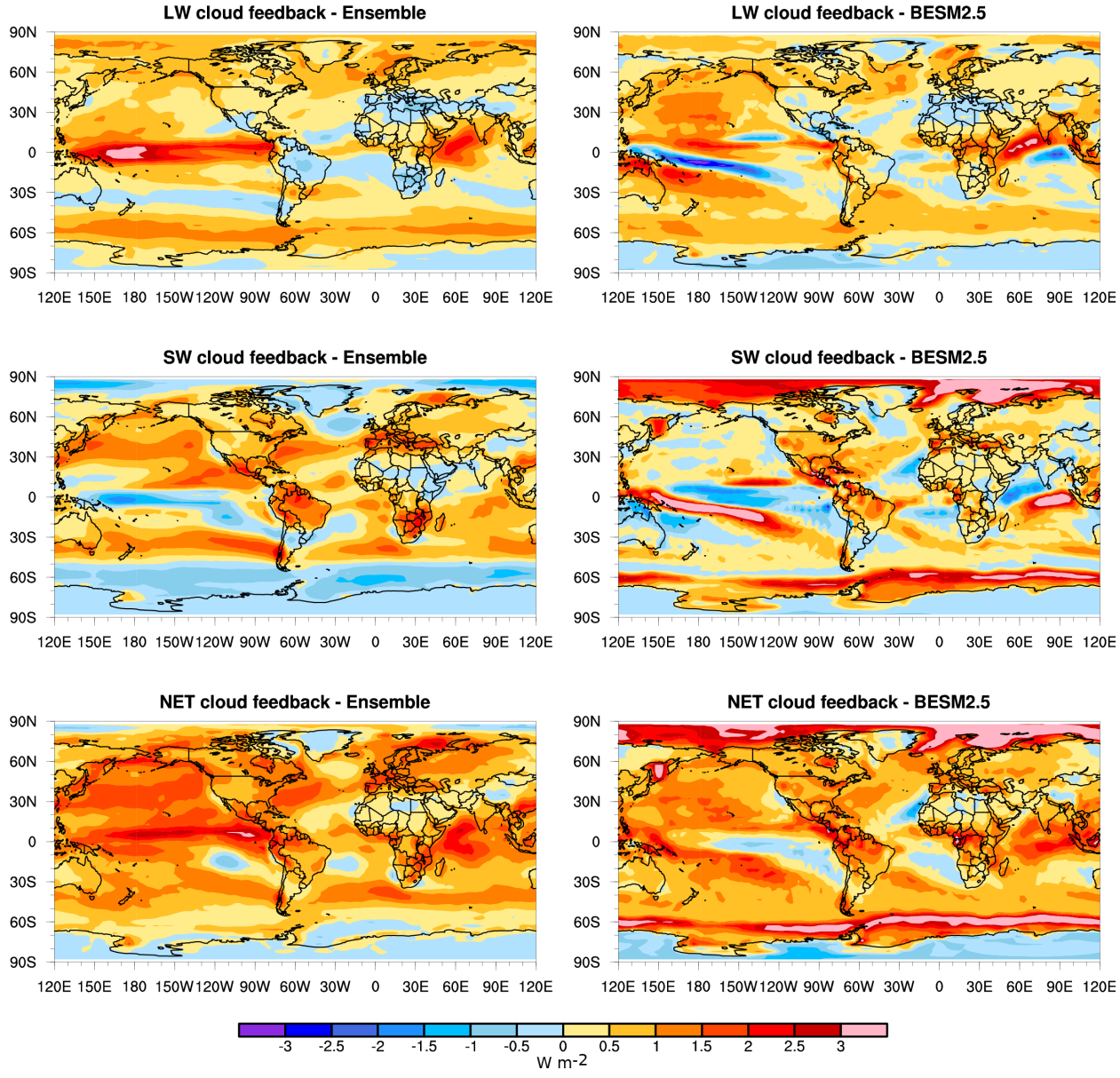

Figure 5. Cloud feedbacks using NCAR radiative kernel for CMIP5 ensemble (left column) and BESM-OA2.5 (right column). Those results are based on the averaged over years 120-150.

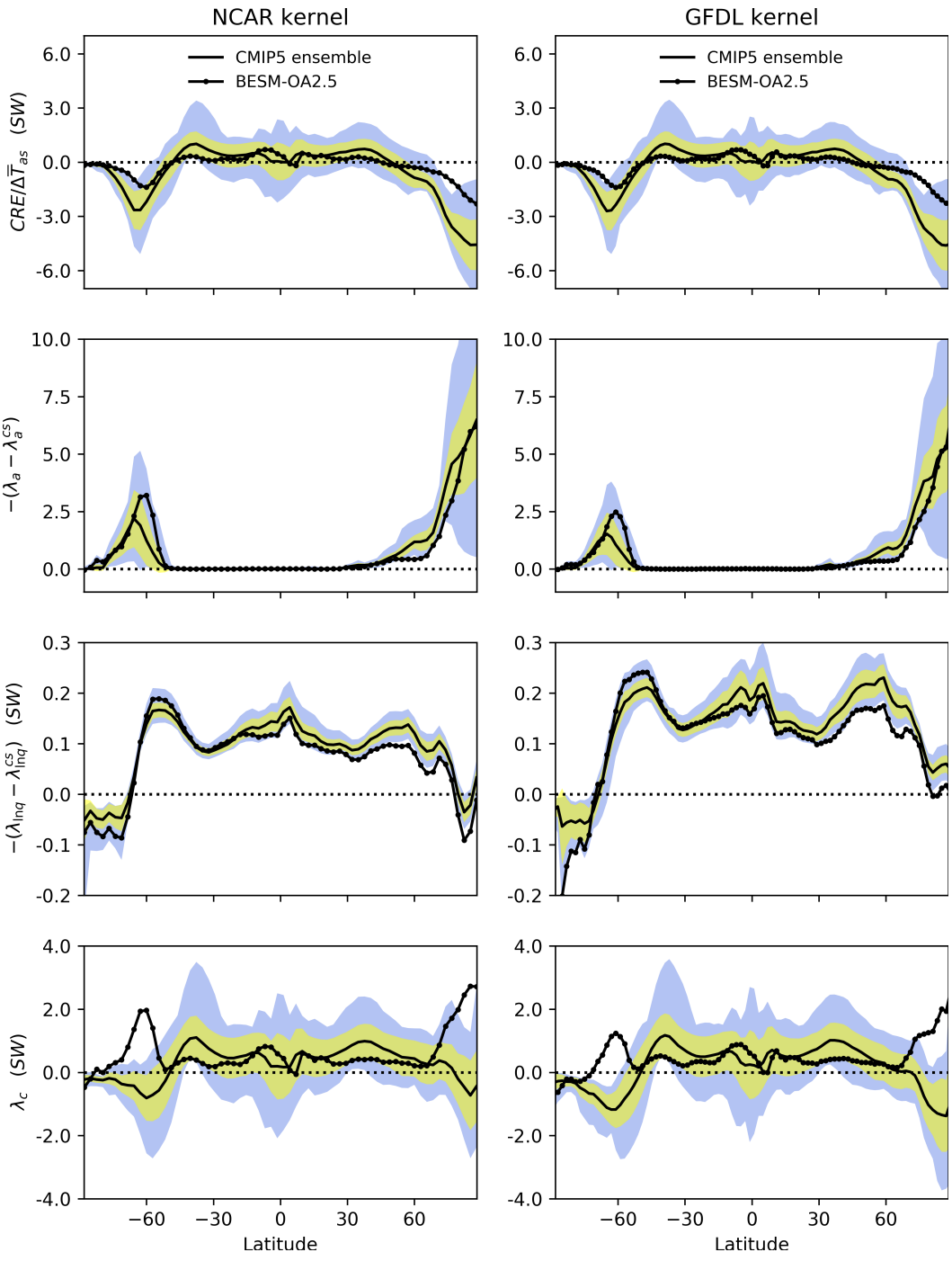

Figure 6. SW Cloud feedback and the albedo and SW humidity feedbacks cloud masking for the CMIP5 multi-model ensemble-mean (solid line) and BESM-OA2.5 (solid line with dots). Inter-model standard deviations for each latitude are in yellow. In blue are the feedback limits based on the maximum and minimum values for each latitude among the models, not including BESM-OA2.5.

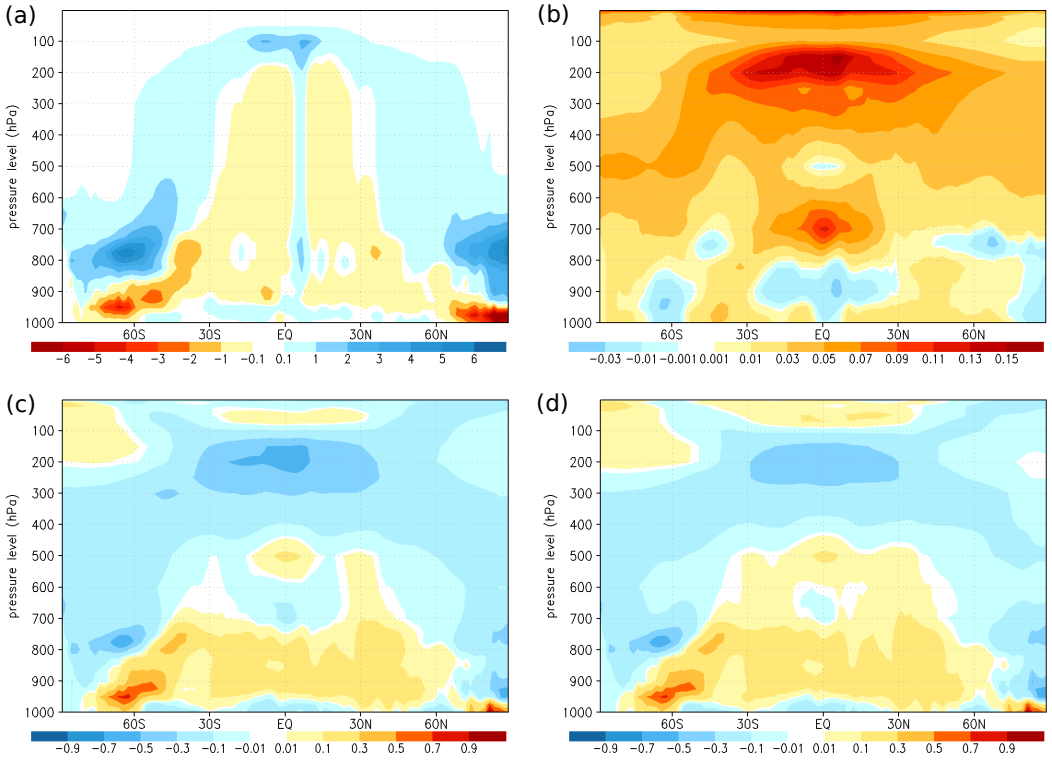

Figure 7. Vertical profiles of the zonal mean of the 4xCO2 - piControl mean difference for the following variables: (a) Cloud fraction, Radiative heating/cooling rate (dT/dt) of (b) shortwave, (c) long wave and (d) sum of shortwave and longwave for BESM-OA2.5.

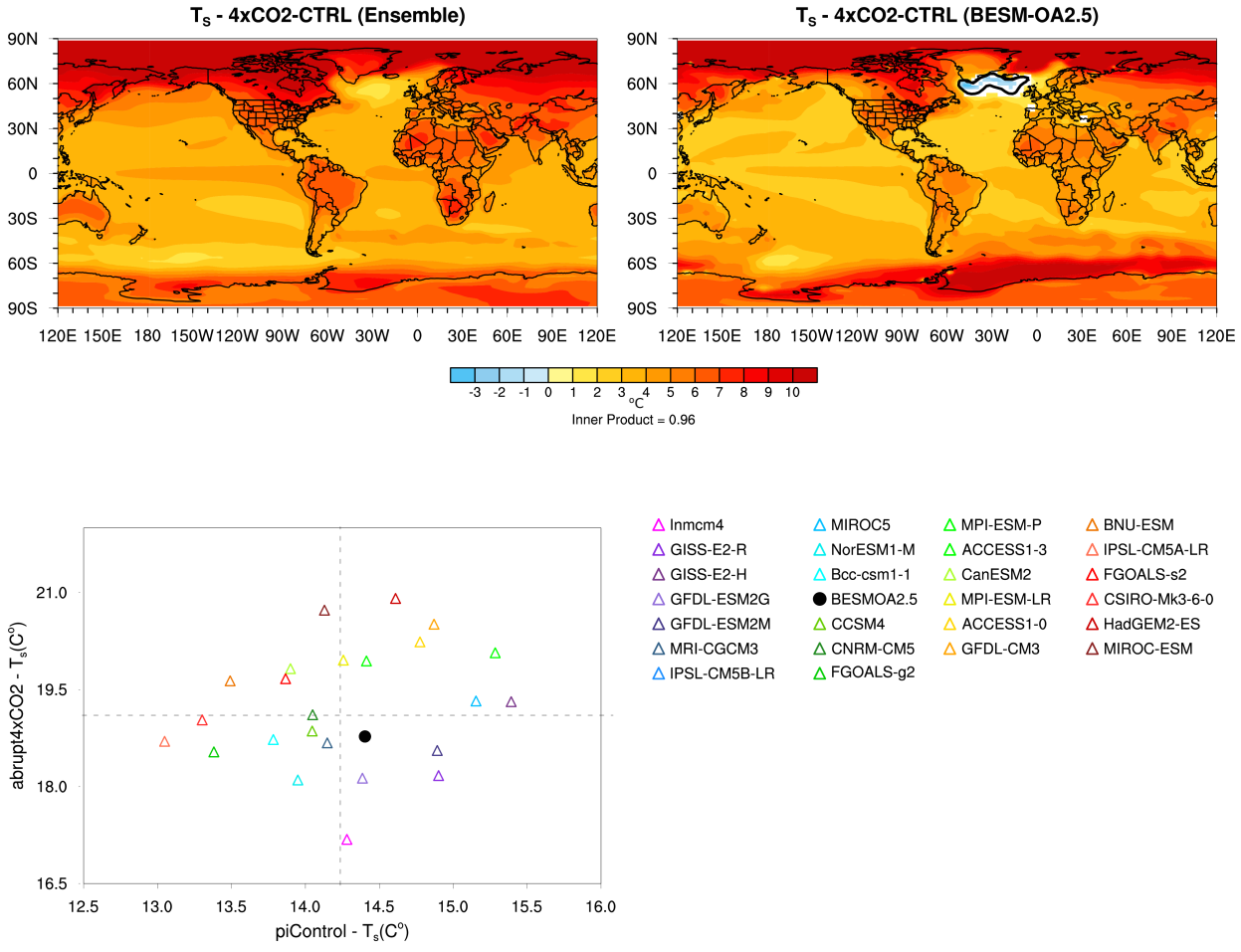

Figure 8. Difference (averaged over years 120-150) of surface temperature between abrupt4xCO2 and piControl simulations in (a) CMIP5 ensemble and (b) in BESM-OA2.5; and (c) scatter plot of global average of surface temperature for the CMIP5 models used in ensemble and BESM-OA2.5 (black dot). Shaded areas in (a) and (b) have level of confidence greater than 90%; the black line represents the isoline of zero temperature difference.

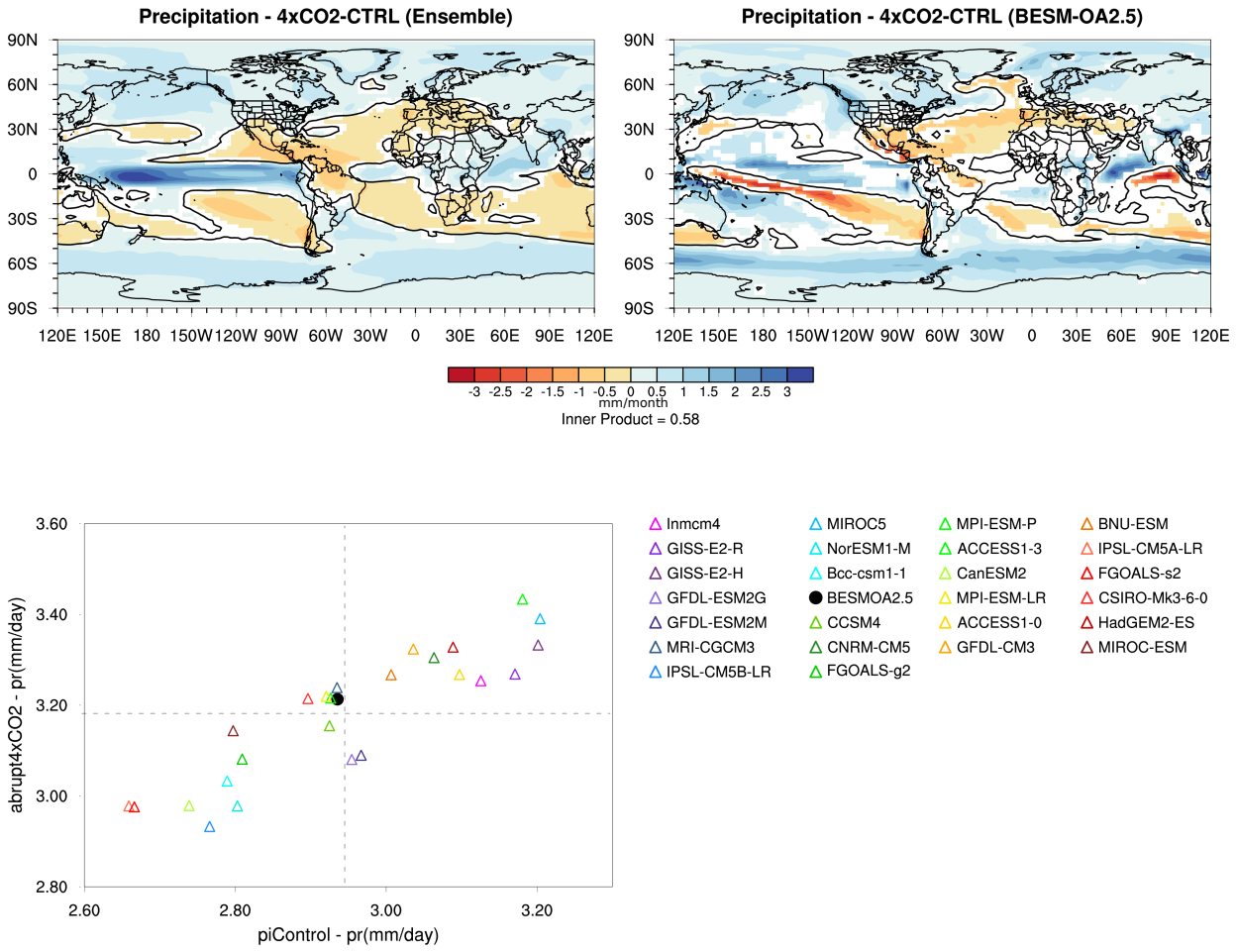

Figure 9. Difference (averaged over years 120-150) of precipitation (in mm/month) between abrupt4xCO2 and piControl simulations in (a) CMIP5 ensemble and (b) in BESM-OA2.5; (c) scatter plot of precipitation global average for CMIP5 models used in the ensemble and BESM-OA2.5 (black dot). Shaded areas in (a) and (b) have level of confidence greater than 90%; the black line represents the isoline of zero precipitation difference.

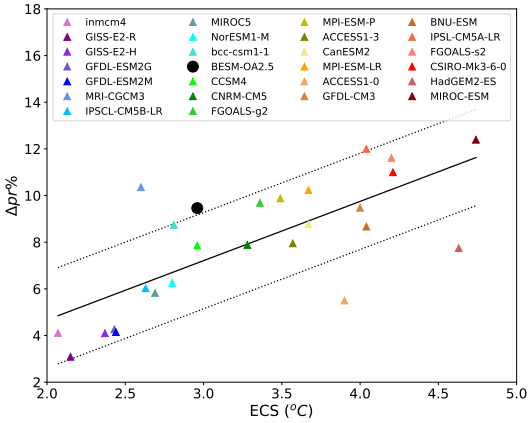

Figure 10. Scatter plot between ECS and $\Delta Pr(\%)$ for all models considered. The solid black line is the linear fit between ECS and perceptual change in precipitation. As in Figure 2, models are sorted according their ECS value. The dash lines represent the error limits considering the residual standard error.

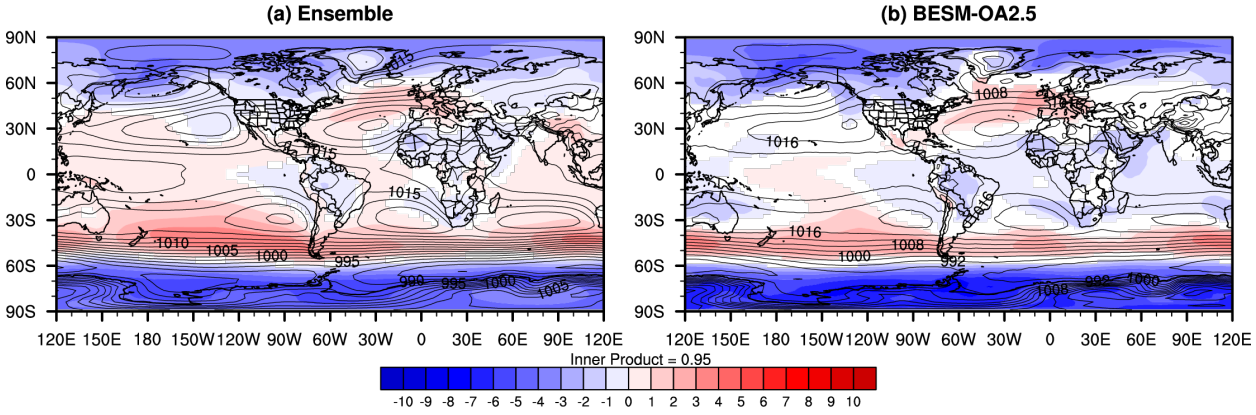

Figure 11. Difference (averaged over years 120-150) of sea level pressure (SLP) in hPa between two scenarios (abrupt4xCO2 minus piControl, shaded), and SLP during piControl (contours) in CMIP5 models ensemble (first column) and BESM-OA2.5 (second column). White areas have level of confidence less than 90%.

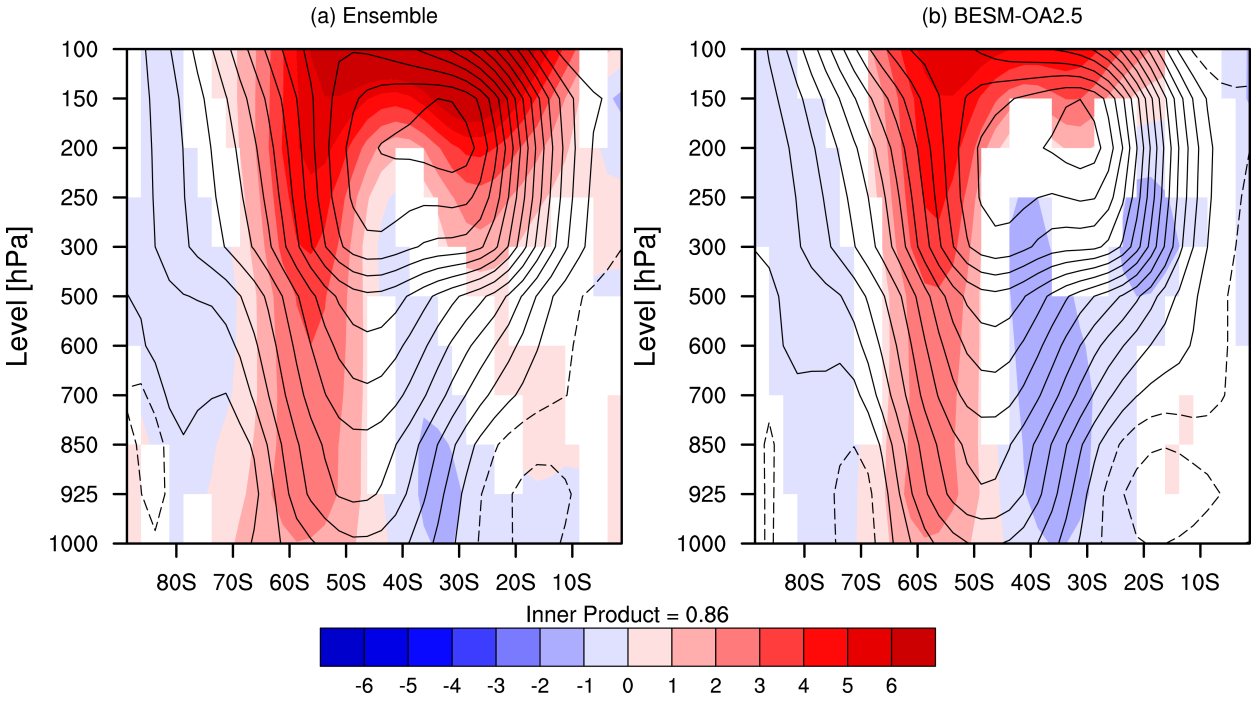

Figure 12. Vertical profile of the difference (averaged over years 120-150) of zonal mean wind (in m/s) between two scenarios (abrupt4xCO2 minus piControl, shaded), and piControl (contours) for (a) ensemble of CMIP5 models and for (b) BESM-OA2.5. White regions have level of confidence less than 90%.

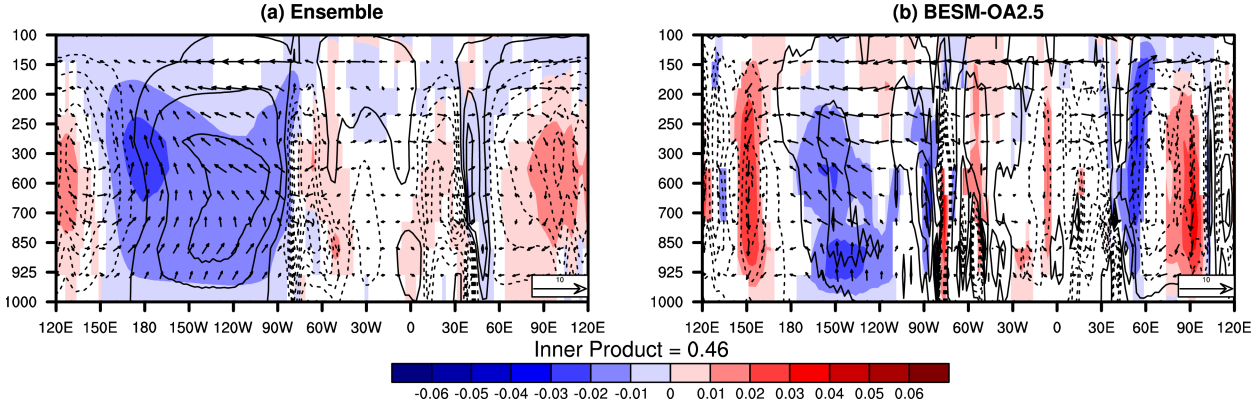

Figure 13. Difference (averaged over years 120-150) between abrupt4xCO2 and piControl for omega (shades) in Pa/s and zonal-vertical winds (vectors), averaged between 5°S and 5°N, for (a) CMIP5 ensemble and (b) BESM-OA2.5. Contours represents the averaged piControl omega in the same region. White areas have a level of confidence less than 90%.

Table 1. Atmospheric physical parameterizations used in BAM (Figueroa et al., 2016) BESM-OA2.5.

Physical Parameterization	BAM	BESM-OA2.5
Shortwave radiation	RRTMG (Iacono et al., 2008)	Clirad (Tarasova and Fomin, 2007)
Longwave radiation	RRTMG (Iacono et al., 2008)	Harshvardhan et al. (1987)
Cloud microphysics	Morrison (Morrison et al., 2005)	Ferrier et al. (2002)
Land surface model	Ibis [Foley et al. (1996) modified by Kubota (2012)]	SSib (Xue et al., 1991)
Planetary Boundary Layer	Modified Mellor and Yamada (1982) scheme	Holtslag and Boville (1993) scheme
Shallow Convection	UW shallow convection (Park and Bretherton, 2009)	Tiedtke (1984)
Deep Convection	Modified Grell and Dévényi (2002) ensemble scheme	Modified Grell and Dévényi (2002) ensemble scheme
Gravity wave	Webster et al. (2003) scheme with low-level blocking	Alpert et al. (1988)
Total Cloud cover fraction	Based on Probability Density Function (PDF)	Slingo (1987)

Table 2. Models belonging to CMIP5 used in this study.

Number	Model	Institution, country
1	ACCESS1-0	CSIRO-BOM, Australia
2	ACCESS1-3	
3	bcc-csm1-1	BCC, China
4	BNU-ESM	BNU, China
5	CanESM2	CCCma, Canada
6	CCSM4	NCAR, USA
7	CNRM-CM5	CNRM-CERFACS, France
8	CSIRO-Mk3-6-0	CSIRO-QCCCE, Australia
9	FGOALS-g2	LASG-CESS, China
10	FGOALS-s2	LASG-IAP, China
11	GFDL-CM3	NOAA-GFDL, USA
12	GFDL-ESM2G	
13	GFDL-ESM2M	
14	GISS-E2-H	NASA-GISS, USA
15	GISS-E2-R	
16	HadGEM2-ES	MOHC, England
17	inmcm4	INM, Russia
18	IPSL-CM5A-LR	IPSL, France
19	IPSL-CM5B-LR	
20	MIROC-ESM	MIROC, Japan
21	MIROC5	
22	MPI-ESM-LR	MPI-M, Germany
23	MPI-ESM-P	
24	MRI-CGCM3	MRI, Japan
25	NorESM1-M	NCC, Norway

Table 3. CO2 Forcing (W m^{-2}) (G), Net Feedback (W m^{-2} K^{-1}) (λ), Climate Response (W m^{-2} K^{-1}) (ΔCRE), and Equilibrium climate sensitivity (K) (ECS) values.

Model	G	λ	ΔCRE	ECS
ACCESS1-0	5.78	-0.74	0.11	3.90
ACCESS1-3	5.71	-0.80	0.27	3.57
bcc-csm1-1	6.72	-1.20	-0.06	2.81
BESM-OA2.5	8.62	-1.45	-0.13	2.96
BNU-ESM	7.45	-0.92	-0.27	4.04
CanESM2	7.51	-1.02	0.16	3.67
CCSM4	7.27	-1.23	-0.15	2.96
CNRM-CM5	7.34	-1.12	-0.19	3.28
CSIRO-Mk3-6-0	5.01	-0.60	0.25	4.21
FGOALS-g2	5.59	-0.83	-0.08	3.36
FGOALS-s2	7.58	-0.90	-0.45	4.20
GFDL-CM3	5.91	-0.74	0.49	4.00
GFDL-ESM2G	5.98	-1.23	-0.21	2.43
GFDL-ESM2M	6.69	-1.37	-0.31	2.44
GISS-E2-H	7.74	-1.64	-0.50	2.37
GISS-E2-R	7.26	-1.69	-0.46	2.15
HadGEM2-ES	5.77	-0.62	0.37	4.63
inmcm4	5.74	-1.38	-0.10	2.07
IPSL-CM5A-LR	6.38	-0.79	0.70	4.04
IPSL-CM5B-LR	5.25	-1.00	0.29	2.63
MIROC5	8.95	-1.66	-0.43	2.69
MIROC-ESM	8.33	-0.88	0.14	4.74
MPI-ESM-LR	8.07	-1.10	-0.06	3.67
MPI-ESM-P	8.39	-1.20	-0.04	3.49
MRI-CGCM3	6.50	-1.25	-0.05	2.60
NorESM1-M	6.19	-1.10	-0.08	2.80
Mean	6.84±1.09	-1.09±0.31	-0.03±0.30	3.30±0.76